Journal of Sedimentary Research

Journal of Sedimentary Research, 2014, v. 84, 513–528
Research Article
DOI: http://dx.doi.org/10.2110/jsr.2014.44

PROVENANCE EVOLUTION DURING ARC–CONTINENT COLLISION: SEDIMENTARY PETROGRAPHY OF MIOCENE TO PLEISTOCENE SEDIMENTS IN THE WESTERN FORELAND BASIN OF TAIWAN

STEFAN NAGEL,[1] SÉBASTIEN CASTELLTORT,[2] EDUARDO GARZANTI,[3] ANDREW T. LIN,[4] SEAN D. WILLETT,[1] FRÉDÉRIC MOUTHEREAU,[5] MARA LIMONTA,[3] AND THIERRY ADATTE[6]

[1]*Department of Earth Sciences, Earth Surface Dynamics, ETH Zürich, Sonneggstrasse 5, 8092 Zürich, Switzerland*
[2]*Department of Geology and Paleontology, University of Geneva, Rue des Maraîchers 13, 1205 Genève, Switzerland*
[3]*Department of Earth and Environmental Sciences, Università di Milano–Bicocca, Piazza della Scienza 4, 20126 Milano, Italy*
[4]*Department of Earth Sciences, National Central University, 300 Jungda Road, Chungli, 16 Taoyuan, Taiwan101*
[5]*Université Pierre et Marie Curie, ISTEP, UMR 71934, Place Jussieu, 75252 Paris Cedex 05, France*
[6]*Institut des Sciences de la Terre, ISTE, Université de Lausanne, CH-1015 Lausanne, Switzerland*
e-mail: stefan.nagel@alumni.ethz.ch

ABSTRACT: **Taiwan is an example of an orogen involving a doubly vergent critical wedge. Critical-wedge theory predicts asymmetrical tectonic development of the pro- and retro- sides of an orogen. Whereas the consequences for exhumation, peak metamorphism, and erosion have been extensively investigated, the implications for sandstone petrography preserved on either side of an orogen have not been adequately documented. Plio-Pleistocene sandstones from the Western Foothills of Taiwan were deposited in a rapidly subsiding foreland basin recording the collision between a volcanic arc and the Asian passive margin. New data on the evolution of sedimentary petrography and clay minerals preserved in Miocene to Pleistocene sandstone of the western pro-foreland basin record the history of Taiwan's orogenesis. Sandstone petrography of the eastern basin on the retro-side of Taiwan's orogenic wedge had been studied previously. Comparison of the provenance record from the western and eastern basins illustrates the opposing signature of unroofing and recycling, held to be characteristic of an asymmetric orogenic wedge. Sandstone petrography can be used in ancient sedimentary basins to complement other indications of the polarity of subduction.**

INTRODUCTION

Sedimentary basins adjacent to orogenic belts contain a long-term record of the geological history of mountain ranges, and therefore provide important constraints on orogenic evolution. Convergent orogens form as wedge-shaped loads on the lithosphere that is variably underthrust or accreted on the overriding plate in the pro-wedge and retro-wedge (Willett et al. 1993). The implications of this asymmetry on erosion, peak metamorphism, and exhumation on the pro- and retro-sides of orogenic wedges have been documented in various orogens, e.g., Southern Alps, New Zealand, Koons (1990), Pyrenees, Puigdefàbregas et al. (1992), and Papua New Guinea, Abbott et al. (1994). In addition, the asymmetrical accretion of material within a critical wedge is also predicted to yield a different signature to be preserved in the sedimentary record of the pro- and retro-foreland basins (Sinclair 2012). According to simple kinematic critical-wedge models for Taiwan (Willett and Brandon 2002), retro-foreland basins should preserve a history of progressive unroofing of deeper crustal material as collision takes place and higher-grade metamorphic rocks are exhumed in the retro-wedge (Barr and Dahlen 1989; Willett 1999). By contrast, the pro-foreland basin record is expected to be that of an increased supply of (recycled) sedimentary fragments that were never deeply buried, as the wedge-top depozones become progressively accreted to the wedge. Such a prediction has never been tested in a real case study (Sinclair 2012).

Taiwan is often considered a type example of a doubly vergent orogenic wedge and has played an important role in the development of theories of critical wedges and steady-state orogens (Dahlen and Suppe 1988; Willett and Brandon 2002; Willett et al. 2003; DeCelles 2011). The accreted and exhumed forearc basin on the eastern side (retro-side) of Taiwan has been the subject of several provenance studies that have illustrated the progressive unroofing history preserved in the petrography of the retro-side sedimentary archives (Liew and Lin 1974; Teng 1979; Page and Suppe 1981; Dorsey 1988; Dorsey et al. 1988; Dorsey and Lundberg 1988). In the pro-foreland basin on the western side of Taiwan there are, however, limited comparable sandstone-petrography and clay-mineralogy studies, with the notable exceptions of Chen et al. (1992), Chen et al. (2000), and Huang et al. (2012). The above studies of Chen et al. (1992) and Chen et al. (2000) documented that the proportion of sedimentary and metamorphic lithic fragments increases upward, with more metamorphic fragments (i.e., slates and metasandstones) in the top foreland succession. In addition, the clay-mineralogy study of Huang et al. (2012) shows that there is an upward increase in illite crystallinity in the foreland succession, suggesting that most illite in the upper foreland succession is sourced from low-grade metamorphic terranes. The vertical change of petrographic compositions and illite crystallinity indicates unroofing of the Taiwan orogen (Chen et al. 1992; Chen et al. 2000; Huang et al. 2012). The above studies did not compare their results with studies from eastern Taiwan, however.

In this study, the results of petrographic compositional analyses (sandstone petrography, clay mineralogy, heavy-mineral assemblages) of a suite of sandstone and mudstone samples from upper Miocene to Pleistocene marine sedimentary strata in the fold-and-thrust belt of the

Published Online: June 2014
 1527-1404/14/084-513/$03.00

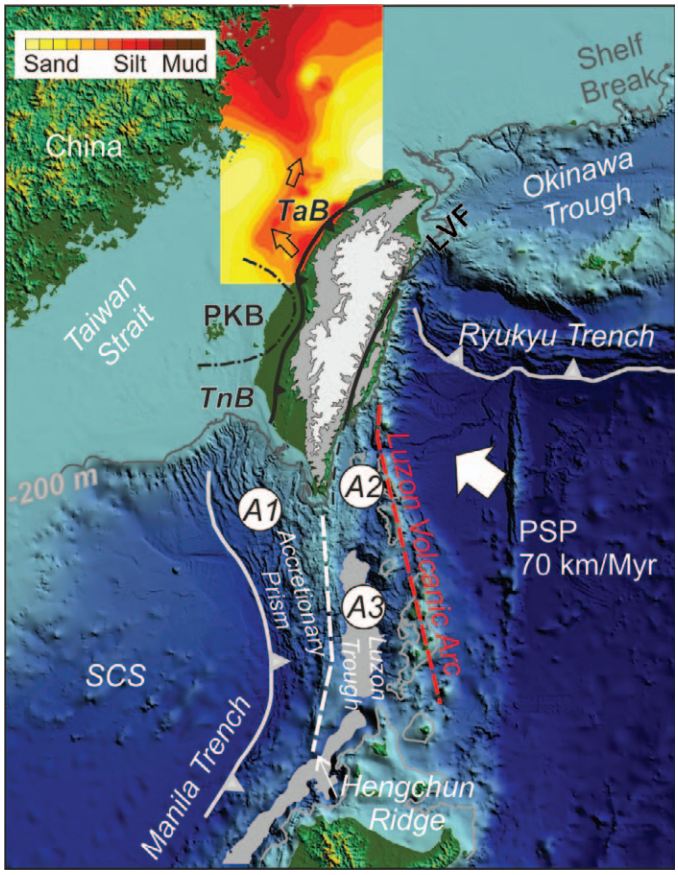

FIG. 1.—Regional bathymetry and simplified tectonic setting of Taiwan. The foreland basin developed on top of a rifted passive margin (Lin et al. 2003). An inherited basement structure, the Peikang Basement High (PKB) (Meng 1971), separates the Northern Taishi (TaB) and Southern Tainan basins (TnB). Numbers (A1–A3) indicate sampling sites for lithic analysis (Yen and Lundberg 2006). Color isopach show distribution of mean grain size in surface sediments in the north, indicating a northward-directed sediment transport of the fine-grained fraction (Huh et al. 2011). PSP, Philippine Sea Plate; SCS, South China Sea; LVF, Longitudinal Valley Fault.

western foreland basin in Taiwan are presented. In combination with published data (e.g., sandstone petrography, clay minerals, heavy minerals) from the Eastern Coastal Range, the study documents how sandstone petrography preserves a signal of the growth of an asymmetrical orogenic wedge.

GEOLOGIC BACKGROUND

Geodynamic Context

Taiwan is situated along the boundary of the Asian passive margin and the Philippine Sea Plate (Fig. 1) and formed by the collision between the Luzon volcanic arc and the passive margin in the late Miocene (Suppe 1981). Two subduction zones have developed. Off NE Taiwan, subduction of the Philippine Sea Plate produces the Ryukyu arc and Okinawa trough, a backarc basin (Sibuet et al. 1995; Sibuet and Hsu 1997). To the Southwest, the Eurasian plate is being subducted eastward along the Manila trench forming the Luzon volcanic arc.

The Asian continental shelf has been a rifted margin since the Cretaceous (Lin et al. 2003), resulting in major subsidence and horst-and-graben formation (Fig. 1, Lin and Watts 2002). The most prominent basement structure of the continental lithosphere, the Peikang basement high (PKB, Fig. 1), divides the western foreland basin into northern and a southern parts (Chou 1973; Tang 1977) and controls structural style and kinematics at the deformation front (Mouthereau et al. 2002; Mouthereau and Lacombe 2006).

Because of the oblique orientation between the volcanic arc and the continental shelf, the collision presumably propagates toward the southwest (Suppe 1984). As a result, the collision is more advanced in the north than in the south, but the orogen eventually has reached a maximum size with nearly constant mountain width and cross-sectional area (Suppe 1981). Because of this constant mountain size for different state of collisional evolution, the orogen is thought to have maintained a balance between tectonic accretion and erosion (“steady state,” Suppe 1981; Stolar et al. 2007).

Synorogenic sediments progressively filled the western foreland basin and unconformably overlie passive-margin sediments with increasing hiatus toward the Peikang High (Yu and Chou 2001; Tensi et al. 2006; Simoes et al. 2007). As the orogenic wedge continuously propagated westward onto the passive margin, flexural subsidence dominated proximal basin development (Castelltort et al. 2011; Nagel et al. 2013). Tectonostratigraphic studies of southwest Taiwan suggest that collision-induced thrust activity in the fold-and-thrust-belt was not active before 5 to 3.5 Ma (Mouthereau et al. 2001; Lock 2007).

Source Terranes

Taiwan consists of four major domains (Fig. 2). From west to east, these domains and their representative lithologies are: The coastal plain (CP) and adjacent offshore areas consist of recent alluvial sediments and Neogene sedimentary sequences not yet deformed by the ongoing collision. The Western Foothills (WF) form a fold-and-thrust belt built up of west-vergent upper Miocene to Pleistocene clastic deposits that overlie older Paleogene to Miocene sequences accumulated on the Asian passive margin. The Central Range (CR), including the Hsuehshan and Backbone Ranges, representing the main segment of the Taiwan orogen, expose Eocene to Miocene low-grade slates and metasandstones of the deformed Asian passive margin (Teng 1990). In the eastern part of the Central Range, the Tananao metamorphic complex includes metasediments (schists, marbles), granitoids, and subordinate metabasites and serpentinites, generally interpreted as a Mesozoic subduction complex reactivated by Plio-Pleistocene arc–continent collision. Metamorphic grade thus increases eastward from very low in the Western Foothills to upper-greenschist facies in the polymetamorphic Tananao Complex (Fig. 2) (Ernst 1983; Jahn et al. 1986). The Coastal Range (CoR) represents the extinct volcanic arc, separated from the Central Range by the Longitudinal Valley Fault (LVF), which is thought to represent the geological suture between the Philippine Sea and Eurasian plates (Fig. 2; Ho 1988). The Coastal Range incorporates Miocene (22 to 5 Ma) sedimentary and volcanic deposits of the accreted Luzon volcanic arc (Dorsey and Lundberg 1988).

METHODS

A set of unweathered samples was collected from several stratigraphic sections along strike in the Western Foothills (Fig. 2). Previous biostratigraphic studies (Chang and Chi 1983; Huang and Huang 1984; Horng and Shea 1996) ensured high-resolution control for sampling and correlations from north to south (Fig. 3). Very fine-grained sandstones (3–4 Φ) were collected for petrography, and mudrocks for clay mineralogy.

Sandstone Petrography

Forty-one thin sections, half stained for plagioclase and K-feldspar and half for calcite, were point-counted (300 to 400 grains per slide) following the Gazzi-Dickinson convention (Dickinson 1970; Ingersoll et al. 1984).

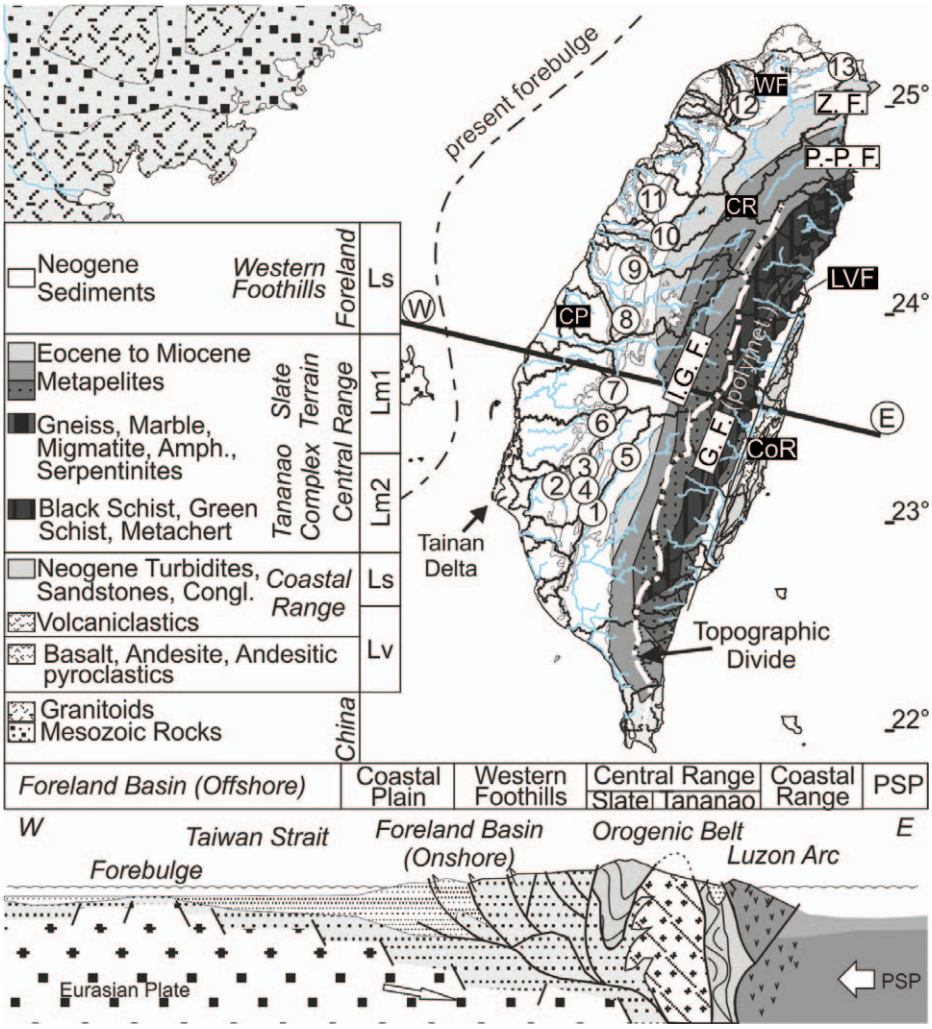

FIG. 2.—Simplified geology of Taiwan with various tectonic units (Chen et al. 1983) and the corresponding lithic fragments for interpretation of the sandstone composition. The Western Foothills (WF) is a fold-and-thrust belt containing Neogene foreland-basin sediments. The coastal plain (CP) and offshore constitutes the undeformed foreland basin. The metamorphic grade in the Central Range (CR) progressively increases from west to east. Higher-grade metamorphic rocks are exposed east of the topographic divide, along the Eastern Central Range. Rivers are blue, corresponding drainage area defined by black lines. Cross section is modified from Molli and Malavieille (2011). Numbers indicate location of stratigraphic sections in Figure 3. Sedimentary lithic fragments include mudstone, shale, siltstone, and argillite clasts. Low-grade metamorphic fragments (Lm_1) include slate, slaty siltstone, and quarzite components, low- to medium-grade metamorphic fragments (Lm_2) are divided into phyllite–schist, phyllitic quarzite, and quartz–micaalbite grains. For a detailed description of lithic types see (Dorsey 1988). Z.F., zeolite facies; P.-P.F., prehnite-pumpellyite facies; l.G.F., lower greenschist facies; G.F., greenschist facies, polymetamorphosed; CoR, Coastal Range; PSP, Philippine Sea plate; LVF, Longitudinal Valley Fault.

Lithic fragments were classified as in Dorsey (1988) to compare her results in the Coastal Range (retro-side) with our results in the western foreland basin (pro-side; Table 1). In order to facilitate comparison with existing petrographic studies on sandstones from the retro-side of the orogen, we use terminology employed by Dorsey (1988) to distinguish sedimentary (Ls) from metamorphic lithic fragments (Lm). Here, low-rank metamorphic fragments (Lm_1) comprise slates, slaty siltstones, and quartzites, whereas medium-rank fragments (Lm_2) correspond to phyllite/schists, phyllitic quartzites, and quartz-mica-albite aggregates. The main source rocks for sedimentary lithic fragments (Ls) is the western Central Range (Hsuehshan Range), dominated by sandstones, shales, and slates. Low-rank metasedimentary fragments (i.e., Lm_1 in Table 1) largely derive from the Eastern Central Range (Hsuehshan and Backbone Ranges), whereas the Tananao schists shed medium-rank metamorphic fragments (e.g., Lm_2, Dorsey 1988).

Heavy-Mineral Assemblages

The heavy-mineral study was performed on 23 samples collected from the Taanchi, Meishan, and Tsengwenchi stratigraphic sections (Fig. 3) and adjacent outcrops covering stratigraphic intervals of late Miocene (12.5 Ma) to late Pleistocene (0.5 Ma). Modern beach sands were also collected in the Tsengwen delta in Tainan (Fig. 2) for comparison with Miocene–Pleistocene samples. Heavy-mineral analysis was performed at ETH Zurich and Università di Milano-Bicocca. Detailed results are provided in Table 4. The samples at ETH Zurich were crushed with a jaw breaker and sieved to separate the 2–4 mm fraction. This fraction was immersed in a solution of 10% acetic acid until all the calcareous cement was dissolved, and the grains were isolated and clean. The fraction was treated between two and five weeks and frequently washed and wet-sieved (0.063–0.4 mm) to periodically remove the mud fraction. After cement dissolution, the heavy minerals were gravimetrically separated from the 0.063–0.4 mm fraction using liquid bromoform (2.88 g/cm^3). The dense fraction was mounted on glass using piperine (refraction index = 1.67). Between 200 and 300 grains were counted per slide using the area method (Galehouse 1971). Heavy-mineral concentration (HMC) was calculated as the volume percentage of total framework grains and total dense grains (Garzanti and Andò 2007). The "Meta-sedimentary Minerals Index" (MMI), based on the relative abundance of chloritoid, staurolite, kyanite, andalusite, and sillimanite (Andò et al. 2013), were calculated for samples where possible. This index varies from 0 in detritus from greenschist-facies to lowermost amphibolite-facies rocks yielding exclusively blue-green amphibole and chloritoid, to 100 in detritus from granulite-facies rocks yielding exclusively brown hornblende and sillimanite, and thus allow us to estimate the average metamorphic grade of meta-igneous and meta-sedimentary source rocks. Values of the ZTR index (Hubert 1962) are also reported on table 4.

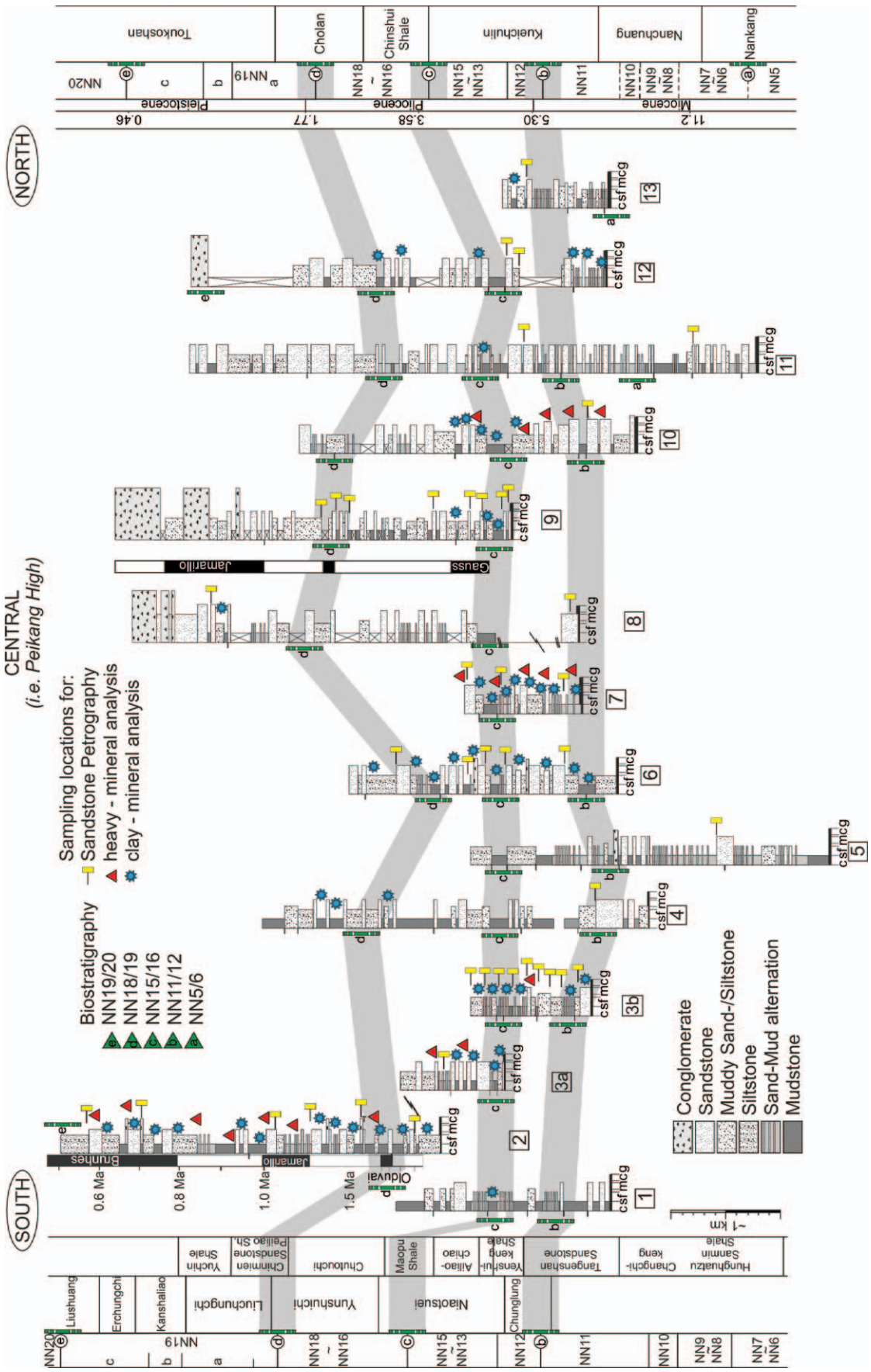

FIG. 3.—Time-stratigraphic chart with the five key biostratigraphic horizons used to study and correlate foreland-basin sediments from north to south (Nagel et al. 2013). The onset of foreland-basin deposition was interpreted dating the basal foreland unconformity (Yu and Chou 2001). The age of the unconformity is estimated to be about 6.5 Ma (Lin et al. 2003). Magnetostratigraphy (additional black/white column) in the Tsengwen–chi (section 2) and Tsaohu–chi (section 9) sections are from Chen et al. (2001). 1) Houkuchi (Huang 1977), 2) Tsengwenchi-West (Chen et al. 2001; Huang 1977), 3) Tsengwenchi–Toll Station (Nagel et al. 2013), Tsengwenchi–Zu Malai Farm (Chi 1978; Nagel et al. 2013), 4) Kueitangchi (Huang 1977), 5) Nantzuhsien (Ting et al. 1991; Yu et al. 2008), 6) Yunshuichi (Wu and Wang 1989), 7) Meishan (Castelltort et al. 2011), 8) Nantou–Chunkungliao (Covey 1984; Nagel et al. 2013), 9) Tsaohuchi (Chen et al. 2001), 10) Taanchi–Huoyenshan (Covey 1984; Nagel et al. 2013), 11) Chuhuangkeng (Huang 1976), 12) Dahanchi (Pan 2011), 13) Pitouchiao (Yu et al. 1999).

TABLE 1.—*Definition of components considered in the ternary diagrams (Dickinson 1985; Dickinson 1970; Ingersoll and Suczek 1979) and classification of metamorphic and sedimentary grains (Dorsey 1988).*

Ternary Diagram	Parameters	Definition
Q-F-L	$Q = Q_m + Q_p$	total quartz grains
	Q_m	monocrystalline quartz
	Q_p	polycrystalline quartz
	$F = P + K$	total feldspar grains (P + K)
	P	plagioclase
	K	potassium feldspar
	$L = L_s + L_{m1} + L_{m2} + L_v$	total lithic fragments
	L_s	sedimentary lithic fragments (e.g. shale, siltstone)
	L_{m1}	very low-rank metamorphic lithic fragments (e.g. slate)
	L_{m2}	low-medium-rank metamorphic rock fragments (e.g. phyllite)
	L_v	volcanic lithic fragments
Q_m-F-L_t	L_t	total lithic fragments + polycrystalline quartz
Q_p-L_v-L_{sm}	L_{sm}	total sedimentary + metamorphic lithic fragments
L_m-L_v-L_s	L_m	total metamorphic lithic fragments ($L_{m1} + L_{m2}$)
L_s-Lm_1-Lm_2	-	-

Clay Mineralogy

Sixty-five mudrock samples were analyzed by X-ray diffraction (XRD) using a Bruker Axis diffractometer (IMP, ETH Zurich) with Cu-Kα radiation and a Ni filter, under a voltage of 40 kV and an intensity of 25 mA. Clay-mineral analyses are based on Kübler (1987). The finely ground powder was first decalcified with 0.2 N HCl, washed with distilled water and centrifuged (five to six times) to obtain a neutral suspension (pH 7–8) and avoid deflocculation. Particles < 2 μm were separated by centrifugation. The < 2 μm solution was pipetted onto a glass slide and analyzed two times following air drying at room temperature and ethylene-glycol solvation for 24 h. Semiquantitative estimates of peak areas of the basal reflections for the main clay-mineral groups were carried out on the glycolizated curve. The mixed-layer fraction was estimated by measuring the position of the composite illite(002)/smectite(003) peak on the glycolizated curve (Moore and Reynolds 1997). The relative error in the estimates of clay-mineral abundances (given in percent) does not exceed 5–10%. Illite crystallinity was measured from the half-height width of the 10 Å peak (Kübler and Jaboyedoff 2000) and calibrated to the scale of Kübler (1987) by measuring selected samples at ETH Zurich and University of Lausanne (correlation methods after Warr and Rice 1994). For that reason, increasing Illite crystallinity (i.e., higher crystallinity) corresponds to the decrease of the half-height peak width, and therefore lower IC values.

RESULTS

Modal Sandstone Compositions

The results of our framework-petrography analysis are shown in Table 2. Ternary diagrams (Q-F-L, L_m-L_v-L_s, and L_s-Lm_1-Lm_2) are shown in Figures 4 and 5 (Dickinson and Suczek 1979; Ingersoll and Suczek 1979; Dorsey 1988; Garzanti and Vezzoli 2003). Also included are literature data from Miocene core samples from Chou (1971, 1976) (X in Fig. 4). The samples are grouped into northern ($> 24^\circ$ N) and southern ($< 24^\circ$ N) locations with reference to the Peikang basement high (PKB, Fig. 1), which divides the Northern Taishi from the Southern Tainan basin (Fig. 1).

In the ternary diagrams, the data split into a Miocene cluster and a Pliocene–Pleistocene cluster, with a large amount of overlap. The evolutionary trend is outlined by the arrows in Figures 4 and 5.

Miocene sandstones contain abundant monocrystalline quartz, quartzite grains, and minor slate fragments, most probably supplied from mainland China. Sandstones from southern Taiwan commonly show abundant bioclastic material (Fig. 6C, G, H). Lower Miocene samples plot close to the quartz corner (average $Q_{90}F_3L_8$) (Figs. 4, 6D). In upper Miocene to Pliocene samples, modal averages are $Q_{66}F_{19}L_{15}$ and $Lm_{67}Lv_6Ls_{27}$.

Upper Pliocene–Pleistocene sandstones have modal averages $Q_{59}F_{18}L_{23}$ and $Lm_{46}Lv_3Ls_{51}$. Slate fragments and bioclastic material are particularly abundant in the upper Pliocene samples (Fig. 6B, 6F), whereas siltstone and mudrock lithic fragments increase upward (Fig. 4B). These correspond to "Type 3" sandstones (little feldspar and abundant sedimentary and metasedimentary lithic fragments) of the Coastal Range (Teng 1979; Dorsey 1988), which were derived mainly from the growing accretionary fold-and-thrust belt of proto-Taiwan during late Pliocene to Pleistocene. Modern sands from southwest Taiwan yield modal averages of $Q_{25}F_{15}L_{60}$ and $Lm_{45}Lv_5Ls_{51}$ in Areas A1 and A2, and of $Q_{25}F_{31}L_{44}$ and $Lm_{22}Lv_{49}Ls_{29}$ in Area A3 (Fig. 1) (Yen and Lundberg 2006).

Figure 5 shows an L_s-Lm_1-Lm_2 ternary diagram for the Western Foothills (West, Fig. 5A) and the Coastal Range (East; Fig. 5B) (Dorsey 1988), indicating that a slight shift in sandstone composition took place simultaneously on both sides of the orogen in late Pliocene–early Pleistocene times. Miocene samples are centered in the Lm_1 corner, whereas younger samples are progressively enriched in sedimentary grains (Fig. 7). In contrast, metamorphic lithic fragments increase upward along the east coast (Dorsey 1988).

Clay Minerals

The dominant clay minerals in the Western Foothills are illite and chlorite, with minor kaolinite, mixed-layer illite–smectite (I/S) and traces of smectite (Fig. 8). To determine the possible sources of Western Foothills mudrocks, literature data (Liu et al. 2010; Wan et al. 2010) are plotted in Figure 8 although generated by different methods. Pleistocene mudrocks have on average 52% illite, 29% chlorite, 11% kaolinite, 8% I–S and scarce smectite (2%) (Table 3). Western Foothills mudrocks plot within the two modern end members "Taiwan rivers" and "Pearl River," suggesting that a comparable situation existed in the past and sediments were derived from both nearby Asia and Paleo-Taiwan. The wider variation compared to modern samples may be caused by different analytical techniques or by physical and/or chemical weathering during transport.

In the south, illite increases up-section, whereas illite–smectite mixed layers decrease simultaneously (Fig. 9). Percent illite in I–S mixed layers also increases up-section in the north. Kaolinite shows small fluctuations, but tends to decrease since early Pleistocene times, whereas it increases in the north (Fig. 9).

TABLE 2.—*Localities and petrographic parameters of sandstone samples from the Western Foothills.*

				Q-F-L [%]			Q_m-F-L_t [%]			Q_p-L_v-L_{sm} [%]			L_m-L_v-L_s [%]			L_s-L_{m1}-L_{m2} [%]			Q_m-P-K [%]		
Sample #	Latitude	Formation	Age Group	*Q*	*F*	*L*	Q_m	*F*	L_t	Q_p	L_v	L_{sm}	L_m	L_v	L_s	L_s	L_{m1}	L_{m2}	Q_m	*P*	*K*
Northern Sections																					
23-1109	24.07163	Toukoshan Bot	NN19b	52.0	9.0	39.0	44.3	9.0	46.7	16.4	4.3	79.3	29.1	5.1	65.8	69.4	22.5	8.1	83.1	6.9	10.0
32-1109	23.9242	Toukoshan Bot	NN19a	64.7	6.8	28.5	50.8	6.8	42.4	32.7	2.5	64.8	38.5	3.7	57.8	60.0	36.2	3.8	88.2	9.1	2.7
22-1109	24.07163	Toukoshan Bot	NN19a	57.5	23.1	19.4	51.6	23.2	25.3	22.7	5.2	72.2	36.0	6.7	57.3	61.4	31.4	7.1	69.0	15.7	15.3
18-1109	24.07761	Cholan	NN16-18	54.2	21.7	24.1	47.8	21.7	30.4	20.4	6.1	73.5	41.0	7.7	51.3	55.6	36.1	8.3	68.8	15.2	16.1
17-1109	24.08102	Cholan	NN16-18	59.1	25.6	15.3	49.4	25.7	24.9	38.4	3.5	58.1	62.3	5.7	32.1	34.0	44.0	22.0	65.8	18.8	15.4
16-1109	24.08379	Cholan bottom	NN16-18	61.5	19.6	18.9	52.2	19.6	28.2	33.0	1.7	65.2	59.7	2.6	37.7	38.7	28.0	33.3	72.7	17.7	9.6
14-1109	24.0841	Chinsui Top	NN16-18	73.2	15.2	11.6	59.7	15.2	25.1	53.5	4.0	42.4	54.3	8.7	37.0	40.5	54.8	4.8	79.7	6.4	13.9
13-1109	24.08547	Chinsui Top	NN16-18	62.8	22.5	14.7	52.4	22.5	25.1	41.5	0.9	57.5	53.2	1.6	45.2	45.9	36.1	18.0	69.9	14.9	15.2
11-1109	24.08653	Chinsui	NN16-18	63.2	22.3	14.6	52.2	22.3	25.5	43.0	2.2	54.8	60.4	3.8	35.8	37.3	39.2	23.5	70.1	15.9	14.0
14-1010	24.855473	Kueichulin Top	NN13-15	66.1	21.6	12.2	56.6	21.7	21.7	43.5	2.9	53.6	79.5	5.1	15.4	16.2	56.8	27.0	72.3	12.4	15.3
13-1010	24.856864	Kueichulin Top	NN13-15	67.7	16.7	15.6	65.7	16.7	17.5	11.1	4.8	84.1	39.3	5.4	55.4	58.5	28.3	13.2	79.7	10.1	10.1
8-1109	24.44466	Kueichulin Bot	NN13-15	62.1	22.6	15.3	54.8	22.7	22.4	31.3	1.5	67.2	76.1	2.2	21.7	22.2	60.0	17.8	70.7	16.8	12.5
31-1109	24.29523	Kuantaoshan Top	NN11-12	62.6	25.0	12.4	58.4	25.0	16.6	25.4	3.0	71.6	82.0	4.0	14.0	14.6	41.7	43.8	70.0	13.9	16.0
11-1010	25.12225	Nanchuang	NN11-12	71.4	3.5	25.1	61.7	3.5	34.8	28.0	12.7	59.3	54.1	17.6	28.2	34.3	55.7	10.0	94.6	4.1	1.4
2-1109	24.46507	Peiliao Sst	NN4-5	57.5	24.7	17.8	51.3	24.7	24.0	25.7	1.0	73.3	66.7	1.3	32.0	32.4	44.6	1.0	67.5	22.8	9.7
Southern Sections																					
63-1010	23.147296	Erchungchi Top	NN19c	58.9	24.7	16.5	52.9	24.7	22.4	26.7	1.1	72.2	40.9	1.5	57.6	58.5	20.0	21.5	68.2	12.5	19.3
59-1010	23.147221	Kanshaliao	NN19c	63.1	16.5	20.4	56.5	16.5	27.0	24.5	1.0	74.5	68.9	1.4	29.7	30.1	50.7	19.2	77.4	8.7	14.0
47-1109	23.139147	Liuchungchi Top	NN19a	57.3	21.0	21.6	53.5	21.1	25.4	14.5	0.0	85.5	63.4	0.0	36.6	36.6	39.4	23.9	71.7	17.6	10.7
51-1010	23.137144	Liuchungchi	NN19a	62.1	25.1	12.9	55.8	25.2	18.9	31.7	1.7	66.7	46.3	2.4	51.2	52.5	37.5	10.0	68.9	12.1	19.1
30-1108	23.13698	Peiliao Shale	NN19a	66.0	9.5	24.5	57.6	9.5	32.9	25.0	0.0	75.0	37.3	0.0	62.7	62.7	29.3	8.0	85.8	9.8	4.4
11-1108	23.56364	Cholan	NN16-18	65.4	17.3	17.3	54.1	17.5	28.4	38.5	1.5	60.0	62.5	2.5	35.0	35.9	33.3	30.8	75.6	15.9	8.5
33-1010	23.385635	Liuchungchi	NN16-18	63.7	6.4	29.9	58.4	6.4	35.2	14.8	0.9	84.3	54.1	1.0	44.9	45.4	32.0	22.7	90.1	4.2	5.7
46-1010	23.139409	Yunshuichi	NN16-18	60.6	23.3	16.1	52.9	23.7	23.4	29.9	2.6	67.5	40.7	3.7	55.6	57.7	28.8	13.5	69.0	8.3	22.6
44-1010	23.127766	Chutouchi	NN16-18	80.4	10.0	9.7	75.2	10.1	14.8	34.0	0.0	66.0	67.7	0.0	32.3	32.3	32.3	35.5	88.2	4.1	7.7
28-1010	23.38337	Yunshuichi	NN16-18	67.1	18.6	14.3	64.3	18.6	17.1	16.1	0.0	83.9	80.9	0.0	19.1	19.1	63.8	17.0	77.6	8.1	14.3
42-1010	23.133343	Chutouchi	NN16-18	72.4	14.7	12.9	68.4	14.8	16.9	23.2	0.0	76.8	81.4	0.0	18.6	18.6	51.2	30.2	82.2	2.9	14.9
26-1010	23.384676	Yunshuichi	NN16-18	42.5	22.4	35.1	33.2	22.5	44.3	20.6	2.2	77.2	40.7	2.8	56.5	58.1	21.9	20.0	59.6	11.7	28.7
41-1010	23.134089	Choutuchi	NN16-18	65.3	16.7	18.0	60.3	16.8	22.9	21.1	2.8	76.1	67.9	3.6	28.6	29.6	46.3	24.1	78.2	1.7	20.1
24-1010	23.382636	Niaotsui Top	NN16-18	60.3	22.6	17.0	53.1	22.6	24.3	29.9	4.6	65.5	47.5	6.6	45.9	49.1	24.6	26.3	70.1	10.7	19.2
04-0109	23.55705	Chinsui Shale	NN16-18	61.9	21.5	16.7	55.6	21.5	23.0	27.4	4.8	67.7	66.7	6.7	26.7	28.6	40.5	31.0	72.1	18.3	9.6
20-1010	23.382529	Niaotsui	NN11-12	69.9	15.9	14.2	67.2	15.9	16.9	16.0	8.0	76.0	52.4	9.5	38.1	42.1	21.1	36.8	80.9	6.1	13.0
38-1010	23.134506	Ailiaochiao	NN13-15	68.0	19.6	12.3	65.9	19.7	14.4	14.3	0.0	85.7	83.3	0.0	16.7	16.7	59.5	23.8	77.0	4.8	18.2
36-1109	23.21431	Ailiaochiao	NN13-15	75.6	20.2	4.2	68.3	20.3	11.4	63.4	14.6	22.0	26.7	40.0	33.3	55.6	22.2	22.2	77.1	11.9	11.0
39-1108	23.24124	Yenshuikeng	NN13-15	77.7	9.2	13.0	68.8	9.3	21.9	40.0	0.0	60.0	86.7	0.0	13.3	13.3	55.6	31.1	88.1	2.2	9.7
38-1108	23.24124	Yenshuikeng	NN13-15	71.3	20.1	8.7	65.9	20.1	14.1	38.3	4.3	57.4	69.0	6.9	24.1	25.9	29.6	44.4	76.7	14.6	8.7
17-0109	23.21671	Yenshuikeng	NN13-15	60.7	26.8	12.5	57.4	27.0	15.7	20.0	10.0	70.0	80.0	12.5	7.5	8.6	28.6	62.9	68.0	23.8	8.2
03-1108	23.56489	Kuantaoshan	NN11-12	58.4	25.1	16.5	54.5	25.1	20.4	19.2	5.1	75.6	52.4	6.3	41.3	44.1	44.1	11.9	68.4	21.1	10.5
11-0109	23.23934	Tangenshan	NN11-12	66.6	26.1	7.4	63.6	26.2	10.2	27.3	3.0	69.7	83.3	4.2	12.5	13.0	56.5	30.4	70.8	22.3	6.9
Tn_01_08	23.06182	Tangenshan	NN11-12	69.5	14.3	16.1	59.9	14.3	25.8	37.4	5.1	57.6	82.3	8.1	9.7	10.5	49.1	40.4	80.7	11.9	7.4
43-1109	23.17893	Changchikeng	NN10-11	57.2	24.4	18.4	49.5	24.5	26.1	29.3	5.1	65.7	61.4	7.1	31.4	33.8	44.6	21.5	66.9	23.1	10.0
CC-01-08	23.07314	Changchikeng	NN10-11	61.5	20.0	18.5	54.3	20.1	25.6	27.7	0.0	72.3	93.3	0.0	6.7	6.7	60.0	33.3	73.0	22.0	5.0

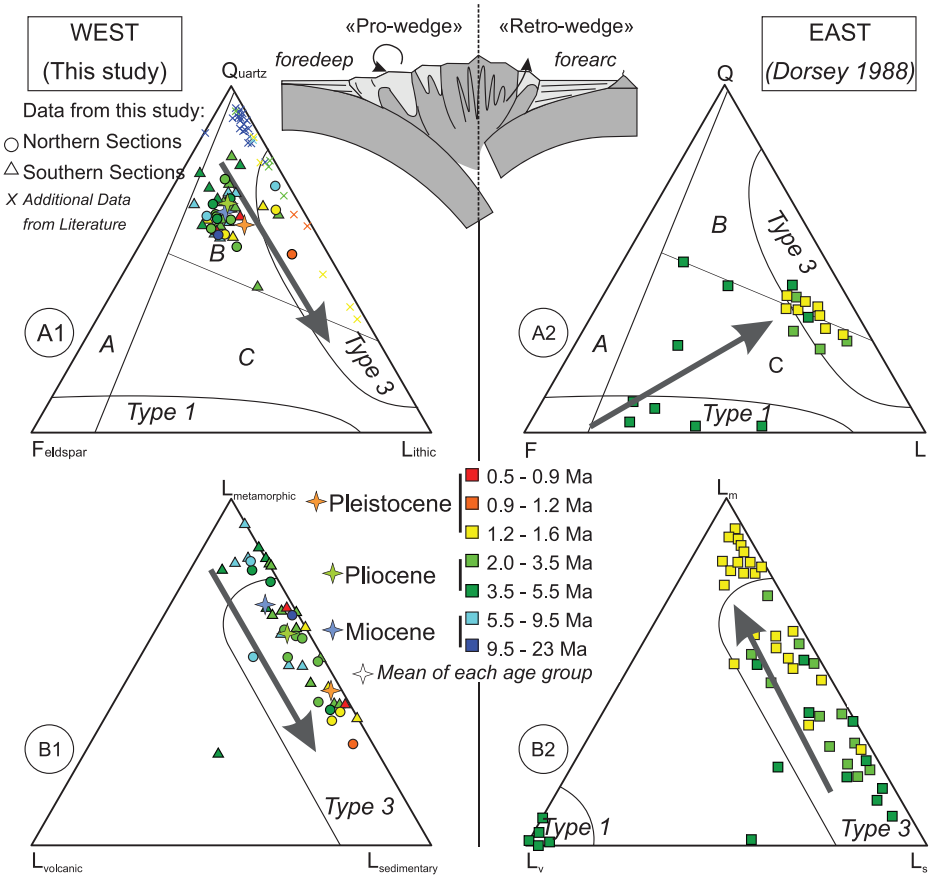

FIG. 4.—Ternary diagrams of sandstones from the Western Foothills (this study, diagrams A1 and B1) and from the Coastal Range (diagrams A2 and B2) (Dorsey 1988; Teng 1979). The petrographic compositions in the western foreland basin show the evolution from passive margin to foreland basin. Arrows indicate evolutionary trends upsection. Color code is based on biostratigraphic data. Provenance fields are from Dickinson and Suczek (1979)(1979) and Ingersoll and Suczek (1979). Miocene samples (marked by X) are from Wu (1967) and Chou (1968). Definition of grain parameters in Table 1 (Dorsey 1988). QFL diagram: A, continental block; B, recycled orogen; C, magmatic arc; Type 1, derived from volcanic source rocks; Type 3, derived from low-grade metamorphic rocks; $L_mL_vL_s$ diagram: A, rifted continental margins; B, mixed magmatic arcs and subduction complexes; C, mixed magmatic arcs and (rifted) continental margins.

Stratigraphic Distribution of Heavy Minerals

In the Taanchi section (North-Central Taiwan) we investigated the Kueichulin Fm (its constituent members of Kuantaoshan Sandstone, Shiliufen Shale, and Yutengping Sandstone), Chinshui Shale (top of the section), and the lower Cholan Fm, spanning the middle Miocene to upper Pliocene (Fig. 10). Most samples are dominated by zircon, tourmaline, and rutile (ZTR values of Hubert 1962; Table 4). Epidote (3–41% tHM) shows a distinct increase up-section in the Chinshui Shale and Cholan Fm. Garnet (12–21% tHM), apatite (5–12% tHM), staurolite (≤ 1% tHM), chloritoid (≤ 2% tHM), and titanite (1–2%tHM) also occur.

In the Meishan section (central Taiwan), we studied the Kueichulin Fm, Chinshui Shale, and lower Cholan Fm, spanning the middle to upper Pliocene (Fig. 10). Most stable minerals (ZTR index 41–86) are associated with apatite (11–31%), garnet (3–30% tHM), epidote (0–7% tHM), chloritoid (1–5% tHM), staurolite (1–3% thM), amphiboles (1–7%), pyroxenes (1–2%), minor kyanite (0.5–1.0%), sillimanite (0.5–2%), and glauconite (> 1%). Garnet increases up-section and reaches maximum relative abundance in the Cholan Fm.

In the Tsengwenchi section (south Taiwan), we analyzed the upper Miocene to upper Pleistocene formations (Tangenshan Sandstone, Yenshuikeng Shale, Ailiaochiao Fm, Chutouchi Fm, Peiliao Shale,

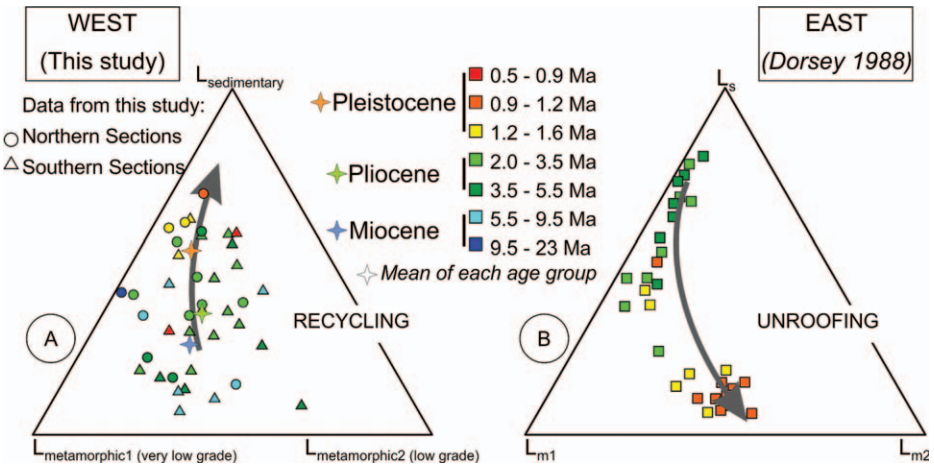

FIG. 5.—Ternary diagrams from the west and east Taiwan forearc and foreland basins respectively. The increase of metamorphic lithic fragments towards younger ages into the forearc basin is interpreted as the progressive unroofing of the metamorphic basement (Dorsey 1988). In contrast, the foreland basin records progressive recycling and mixing of the sedimentary cover. Arrows indicate evolutionary trends upsection. Color code is based on biostratigraphic data (see Nagel et al. (2013) for extended reference list).

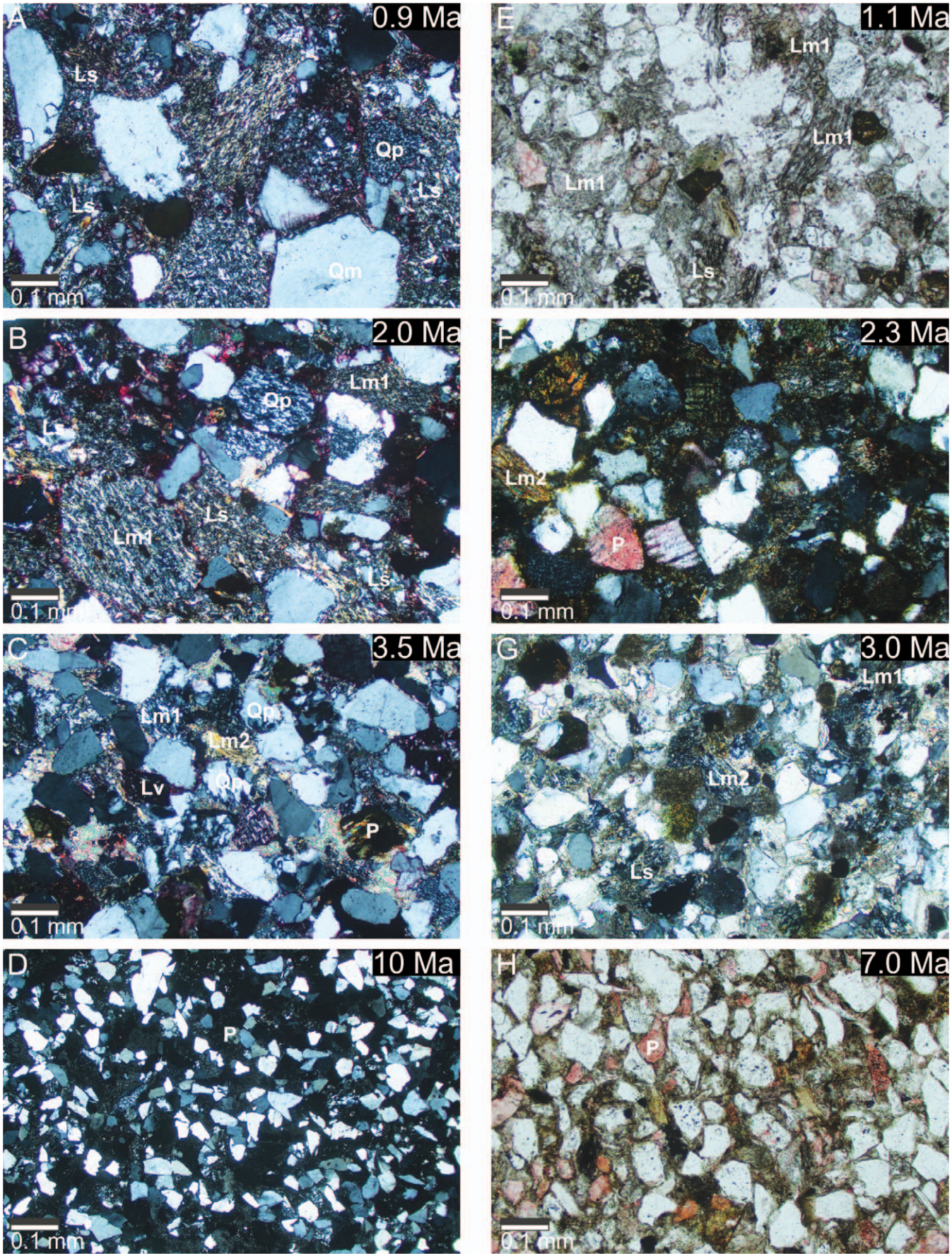
A
0.9 Ma
Ls
Qp
Ls
Ls
Qm
0.1 mm
E
1.1 Ma
Lm1
Lm1
Lm1
Ls
0.1 mm
B
2.0 Ma
Lm1
Qp
Ls
Ls
Lm1
Ls
0.1 mm
F
2.3 Ma
Lm2
P
0.1 mm
C
3.5 Ma
Lm1
Qp
Lm2
Lv
Qp
P
0.1 mm
G
3.0 Ma
Lm1
Lm2
Ls
0.1 mm
D
10 Ma
P
0.1 mm
H
7.0 Ma
P
0.1 mm

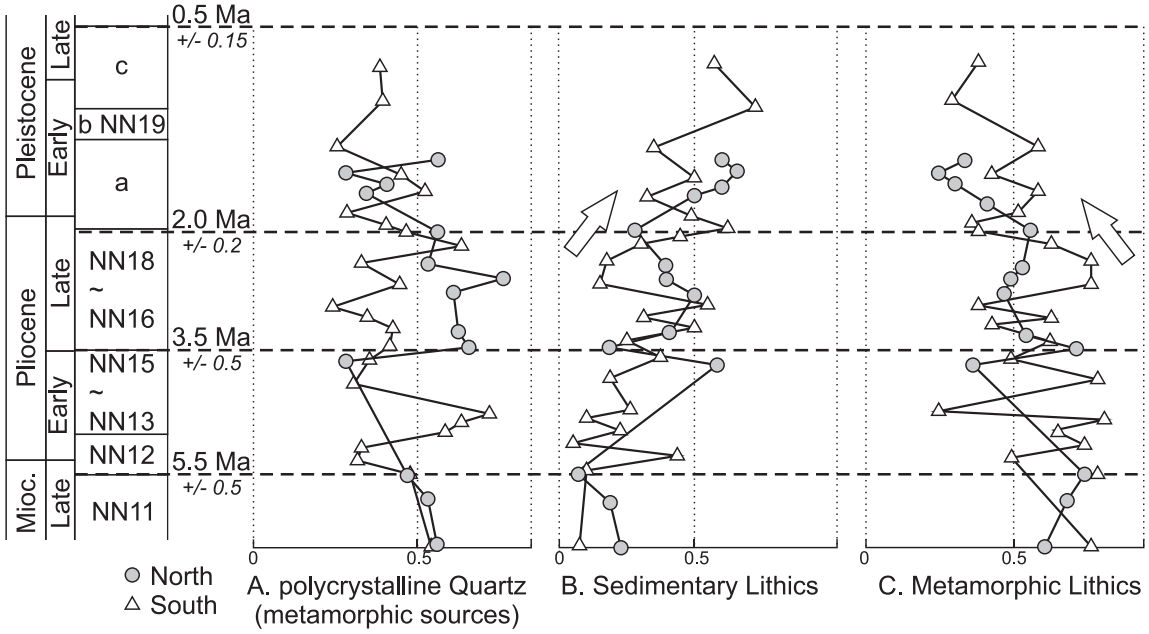

FIG. 7.—Stratigraphic distribution of petrographic ratios in samples from main grain types (see Table 1). Composite sections from the north (Tsaohuchi, Taanchi, Chuhuangkeng) and south (Tsengwenchi, Yunshuichi, Meishan). Progressive increase of sedimentary lithic fragments and simultaneous decrease in metamorphic lithic fragments indicated from late Pliocene on. Metamorphic index is based on methods in Garzanti and Vezzoli (2003).

Yunshuichi Fm, Liuchungchi Fm, Erchungchi Fm, and Liushuang Fm) (Fig. 10). Stable minerals (ZTR index 34–75) are associated with garnet (10–33%), decreasing slightly in relative abundance from the Peiliao Shale to the Liushuang Fm. Apatite (4–30%) is most abundant in the upper Ailiaochiao and Chutouchi fms., and decreases up-section. Chloritoid (1–9.5%) and staurolite (1–4%) are more common in the lower part of the section. Minor titanite (< 1%), amphiboles (1–11%), pyroxenes (1–4%), epidote (1–6%), kyanite (1–2%), and sillimanite (1–1.5%) occur. Glauconite (< 1%) was observed only in the Yenshuikeng and Tangenshan fms.

The main composition of the three sections analyzed does not change markedly over the period recorded. The southwestern part shows an upward decrease in garnet, epidote, and chloritoid, in contrast to a constant sediment supply to the central parts, which is consistent with increasing detritus from the uplifted sedimentary foothills of southwestern Taiwan. The relatively homogeneous composition of the southwestern section, and the very minor increase in metamorphic assemblages observed in the younger formations (staurolite, kyanite, and sillimanite), reflects a stable fluvial drainage pattern in the southwestern part of the source area. In contrast, the northernmost section analyzed (e.g., Taanchi) shows a distinct upward increase in epidote–chloritoid grains relatively early from early Pliocene (Kuechulin Fm) upsection, which indicates a progressive cutting by erosion into greenschist-facies metamorphic source rocks.

DISCUSSION: PROVENANCE EVOLUTION DURING ARC–CONTINENT COLLISION

The provenance evolution of the western foreland basin of Taiwan is marked by the oblique collision between the Luzon volcanic arc and the Asian passive margin, producing distinct sandstone and clay-mineral compositions on different sides of the orogen. In the late Miocene to Pliocene early stages of collision (5.5–3.5 Ma; Fig. 11A), the area of Taiwan was located on a rifted passive margin, which received clastic detritus from the Asian continent. An increase in feldspar (i.e., plagioclase) and volcanic rock fragments in early Pliocene forearc sediments indicate onset of collision with the Luzon arc (Dorsey 1988). Growth of the Taiwan orogen is heralded in upper Pliocene to lower Pleistocene deposits on both sides of the island by clasts from greenschist-facies rocks exhumed in the center of the orogenic wedge (Fig. 11B) (Yamato et al. 2009). This signal is blurred in the west by recycling of older foreland deposits but is confirmed by the appearance of pyrrhotite, diagnostic of provenance from the Central Range, as recorded in the Yunshui-chi section in south-central Taiwan around 2.4 Ma (Horng et al. 2012).

←

FIG. 6.—Selected sandstones representing major changes in clast composition from north (Tsaohu-chi, 9 in Fig. 2) and south (Tsengwen-chi, 2/3 in Fig. 2 and Yunshui-chi, 6 in Fig. 2). Thin sections were stained for plagioclase (albite with no color, anorthite increasingly red) and K-feldspar (yellow to brownish colored) **A)** Abundant sedimentary lithic fragments (siltstones, containing silt- and fine sand-size subgrains of quartz, feldspar, minor lithic fragments, and shales, very fine-grained clayey matrix with microscopic planar-bedding fabric) and minor Lm1 fragments, Toukoshan Fm., Tsaohuchi (crossed nicols), **B)** Upper Pliocene sandstone recording increased fine-grained sedimentary fragments, Cholan Fm., Tsaohu-chi (crossed nicols), **C)** The upper part of the Chinshui Shale, with abundant polycrystalline quartz and traces of volcanic lithic fragments, Tsaohu-chi (crossed nicols), **D)** Upper Miocene sandstone dominated by monocrystalline quartz and traces of volcanic fragments and feldspar, Nanchuang Fm., Keelung (crossed nicols), **E)** The Kanshaliao Fm. records abundant slaty siltstones grains (Lm_1) in contrast to the northern section (see Part A), Tsengwen-chi (parallel nicols), **F)** Very few Lm_2 grains (phyllite schists contain clear micas commonly alternating with thin layers of highly recrystallized quartz in a strongly preferred planar foliation) are present in the younger sections, Peiliao Shale, Tsengwen-chi (crossed nicols), **G)** Yunshuichi Fm. with a mixed composition of abundant sedimentary and metamorphic grains, Yunshui-chi (crossed nicols), **H)** Sandstone from the upper Miocene Tangenshan Fm. Note the muddy matrix and abundant Plagioclase (red stained). Tsengwen-chi (parallel nicols).

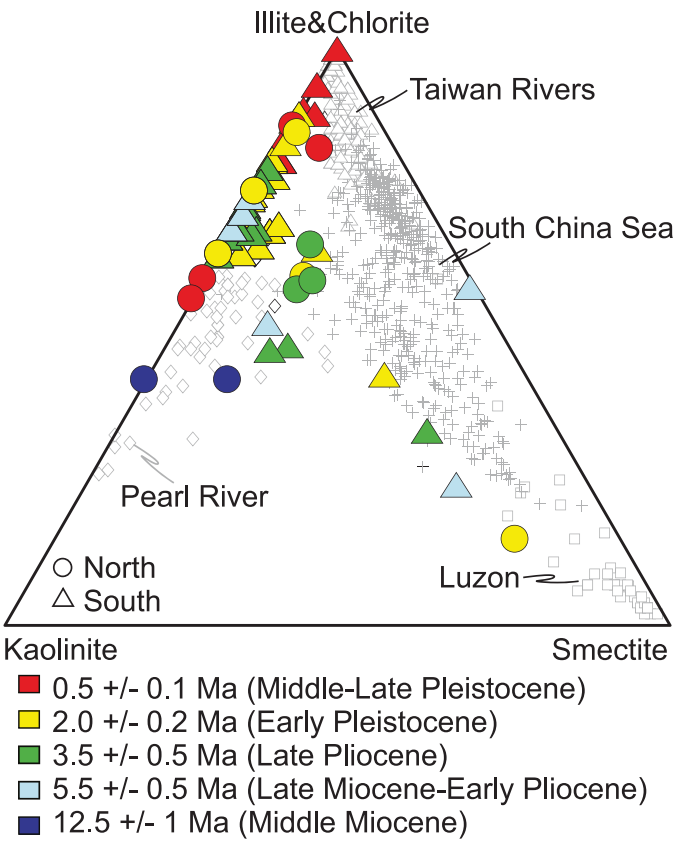

FIG. 8.—Comparison of clay-mineral assemblages in mudstones from the Western Foothills, divided into north and south relative to the location of the Peikang High. Color code is based on five key biostratigraphic horizons (see Fig. 3). Literature data with source areas interpreted from modern river and offshore samples, compiled from Wan et al. (2010) and Liu et al. (2010), although generated by different methods.

Recycling of material in the orogenic wedge integrated all processes that led to an incorporation of older material into younger geological units. The dominant mechanism of accretion and deformation in the fold-and-thrust belt of western Taiwan is best explained by thin-skinned tectonic processes, where a series of west-verging thrust faults run into different décollement surfaces linked by ramps (Davis et al. 1983; Suppe 1983; Suppe and Namson 1979). Material is further incorporated by the forward propagation of thrust faults, which widened the thrust belt as the deformation front stepped into the foreland basin. These large-scale tectonic processes led to a dilution by erosion of uplifting anticlines in the foothills.

In our schematic geodynamic model (Fig. 11), we envisage an eastward shift of the focus of exhumation associated with strong asymmetry of the growing orogenic wedge. Asymmetric exhumation is recorded in the east by higher sediment accumulation rates and shorter lag times, starting somewhere between 2.9 and 1.9 Ma (Kirstein et al. 2009). As a result, cover strata eroded from the topmost parts of the accretionary prism supplied sedimentary detritus into the retro-side of the prism (i.e., the forearc basin).

A similar mechanism, with lateral growth of the deformation front gradually preventing metamorphic detritus from reaching the foreland, may also explain the sedimentary record of other foreland basins. This is consistent with sandstone modal compositions becoming progressively dominated by sedimentary clastic influx since 17 Ma, as observed in the Himalayan foreland-basin succession (Najman et al. 2009; White et al. 2002). In Taiwan, the upward increasing influx of sedimentary detritus is synchronous with increased sediment accumulation rates (Chang and Chi 1983), increased tectonic subsidence (Lin et al. 2003; Tensi et al. 2006), retrogradational facies belts recorded in the Western Foothills (Nagel et al. 2013), and accelerated exhumation and cessation of major volcanism in the Coastal Range (Kirstein et al. 2009; Yang et al. 1995). These phenomena are related to the initial collision and mountain building in Taiwan.

In the late Pliocene to Pleistocene, rapid uplift and unroofing of the Central Range led to exposure of progressively higher-grade metamorphic rocks. This is recorded by increasing metamorphic lithics (Figs. 5B, 11D) in the east (Dorsey 1988), where the tectonic setting of the previous forearc basin was similar to the present day, with a paleo-Hengchun ridge acting as a barrier shielding the North Luzon Trough from sediment influx derived from Asia (Fig. 11E) (Yen and Lundberg 2006). This scenario is generally consistent with geodynamic models by Yamato et al. (2009) and Kaus et al. (2008).

The sandstones from the Western Foothills exhibit a systematic increase in lithic fragments at the expense of quartz and feldspar (mainland China source areas) (Fig. 7), which reflects the change from mature passive-margin to foreland-basin sedimentation. The Central Range of Taiwan is dominated by shales and slates shedding abundant illite and chlorite (Liu et al. 2008). A comparable situation existed in the past, providing large amounts of illite and chlorite to the strata now exposed in the Western Foothills (Fig. 8). Up-section, illite increases and I–S mixed layers decrease, which is opposite to the effect of burial diagenesis (Moore and Reynolds 1997) (Fig. 9). Also, in boreholes in southwest Taiwan (Manius et al. 1985) and NW Taiwan (Huang et al. 2012), illite increases up-section, indicating its detrital rather than diagenetic origin. Because deeper stratigraphic units of the Western Foothills are not involved in the fold-thrust-belt deformation (Lock 2007), the increasing illite crystallinity up-section conclusively proves that higher-grade metasedimentary rocks have been progressively unroofed and supplied from the Taiwan orogenic complex in the hinterland since the late Pliocene (Fig. 9). Illite-crystallinity values in detrital samples indicate temperatures resulting from 6–10 km of burial (200–300°C), which is consistent with late Miocene to early Pliocene onset of collision (Lin et al. 2003) preceding influx of crystalline illite by 3–2 Ma at least.

Increasing illite crystallinity in the northern foothills (pro-side) suggests that unroofing of the schist belt progressed at a relatively constant rate through time. A similar illite–crystallinity trend was observed in mudrocks from the east coast (retro-side) (Dorsey et al. 1988). The progressive increase in illite crystallinity in the Western Foothills is consistent with progressive deepening of erosion into metamorphic rocks, as revealed by up-section increase in epidote and chloritoid in the Taanchi section (Fig. 9). Conversely, the lack of an obvious increase in illite crystallinity in the southern foothills was caused chiefly by recycling of sedimentary cover, as indicated by the much greater influx of sedimentary detritus (Figs. 7, 9). Clay-mineral trends on the pro-side of the orogen confirm progressive unroofing of the Western Foothills, but not as clearly as on its retro side.

CONCLUSIONS

Our study provides new insights into the sedimentary record of an active arc–continent collision, and specifically focuses on the asymmetry of the provenance signal preserved in foreland-basin successions deposited along the pro-side and retro-side of a doubly vergent orogenic wedge.

In the pro-foreland basin (i.e., Western Foothills), the increase in sedimentary lithic fragments upsection, starting in the late Pliocene, provides evidence of recycling of sedimentary strata, as predicted by theories of asymmetrical erosion of doubly vergent orogens with shallow trajectories of burial and exhumation in the frontal pro-wedge, but deeper

TABLE 3.— *Clay-mineral contents and parameters in Miocene to Pleistocene mudstone samples from the Western Foothills.*

Sample #	Formation	Latitude	*% Illite*	*I% /S*	*% Chlorite*	% Kaolinite	*% Smectite*	*Illite Crystallinity* (°Δ2θ)	*Illite Chemistry*	% Illite in I/S
12-1010	Nanchuang	25.121151	-	-	-	-	-	0.25	0.21	-
16-1010	Nanchuang	24.948509	-	-	-	-	-	0.27	0.42	-
8-1010	Nanchuang	24.948371	33	5	21	32	9	0.22	0.26	82
15-1010	Nanchuang	24.948371	34	4	20	42	0	0.26	0.50	78
3-1010	Cholan, Bottom	24.848814	46	4	21	18	11	0.25	3.39	71
5-1010	Toukoshan, Bottom	24.841824	44	1	25	30	0	0.22	0.32	68
4-1010	Toukoshan	24.83977	43	7	19	30	0	0.20	0.71	95
9-1010	Peiliao Shale	24.69798	56	3	23	18	0	0.32	0.42	80
7-1109	Cholan, Bottom	24.46384	21	13	10	10	45	0.37	0.59	82
17-1010	Kueichulin, Top	24.293574	52	1	16	20	11	0.17	0.30	82
28-1109	Cholan, Bottom	24.28943	49	0	24	27	0	0.22	0.43	54
29-1109	Chinsui Top	24.28943	48	0	21	18	13	0.21	0.84	52
14-1109	Chinsui Shale, Top	24.0841	-	-	-	-	-	-	-	-
15-1109	Chinshui Shale, Top	24.08379	48	3	25	15	10	0.25	1.37	61
20-1109	Cholan, Top	24.07749	42	3	44	9	1	0.27	0.65	76
21-1109	Toukoshan, bottom	24.07163	38	10	43	9	0	0.26	0.91	87
34-1109	Toukoshan, Bottom	23.92444	48	2	38	8	4	0.28	0.29	77
7-1108	Chinshui Shale	23.56901	46	17	20	17	0	0.25	0.96	82
2-1108	Kuantaoshan	23.56489	52	5	25	19	0	0.52	0.82	83
10-1108	Cholan, Top	23.56453	78	3	7	12	0	0.46	0.99	73
12-1108	Cholan	23.56364	76	7	9	7	0	0.59	-	78
40-1108	Kueichulin	23.56325	49	16	19	16	0	-	0.57	63
8-0109	Kueichulin Top	23.55744	56	5	27	12	0	0.30	0.63	88
9-0109	Kueichulin Top	23.55744	38	6	35	21	0	0.27	0.76	82
4-0109	Chinsui, Bottom	23.55705	51	4	25	20	0	0.24	0.68	72
12-0109	Kueichulin	23.5558	38	8	17	11	27	0.28	0.66	60
4-1108	Shiliufen Shale	23.55534	32	14	14	11	30	0.27	0.26	75
36-1010	Liuchungchi, Top	23.38512	56	1	28	15	0	0.43	0.59	47
29-1010	Yunshuichi	23.384837	43	11	27	16	3	0.52	0.45	71
25-1010	Yunshuichi, Bottom	23.38391	54	1	26	19	0	0.34	0.72	47
27-1010	Yunshuichi	23.38337	50	8	25	17	0	0.51	0.38	51
32-1010	Liuchungchi	23.383244	49	9	30	12	1	0.49	0.72	77
23-1010	Niaotsui, Top	23.382636	36	14	22	18	10	0.41	0.91	76
19-1010	Chunlun	23.382559	67	9	1	0	23	0.47	1.23	54
18-1010	Chunlun	23.381765	35	16	24	18	7	0.52	1.30	77
30-1010	Yunshuichi, Top	23.381748	40	4	22	13	21	0.41	0.25	70
22-1010	Niaotsui	23.380514	38	6	25	21	9	0.58	1.16	56
13-0109	Yenshuikeng, Top	23.23989	46	15	24	15	0	0.30	0.15	82
14-0109	Maopu/Chutouchi	23.23342	47	4	31	18	0	0.33	0.18	74
19-0109	Ailiaochiao	23.21417	50	5	29	16	0	0.26	0.79	71
38-1109	Ailiaochiao Top	23.21129	42	19	25	14	0	0.47	0.43	80
64-1010	Erchungchi, Top	23.147296	56	7	31	6	0	0.50	0.59	70
58-1010	Kanshaliao	23.147163	63	7	30	0	0	0.39	0.56	68
62-1010	Erchungchi	23.146761	62	14	17	6	0	0.34	0.24	79
55-1010	Kanshaliao	23.145883	47	23	20	9	1	0.48	0.74	81
57-1010	Kanshaliao	23.145883	51	17	23	8	0	0.42	0.55	74
56-1010	Kanshaliao	23.141588	55	2	36	6	1	0.37	0.36	64
26-1108	Peiliao Shale	23.14075	66	4	24	7	0	0.41	0.56	67
27-1108	Yuching Shale	23.14075	53	12	21	14	0	0.26	0.22	47
45-1010	Yunshuichi	23.140009	40	10	28	14	8	0.44	0.89	78
47-1010	Yunshuichi, Top	23.139147	47	6	29	15	3	0.52	0.81	68
48-1010	Liuchungchi	23.13889	49	3	30	16	3	0.41	0.63	70
46-1109	Liuchungchi	23.13869	44	4	33	14	4	0.28	1.18	78
45-1109	Yunshuichi	23.13814	56	4	29	11	0	0.19	0.63	84
50-1010	Liuchungchi	23.138106	44	10	27	11	8	0.43	0.73	60
32-1108	Peiliao Shale	23.13698	47	5	33	15	0	0.31	0.58	77
52-1010	Liuchungchi	23.135697	52	3	35	10	0	0.51	0.68	59
37-1010	Ailiaochiao	23.134506	46	13	24	15	2	0.35	0.51	72
TWC-3808	Liushuang	23.13439	45	2	49	4	0	0.19	-	79
39-1010	Maopu	23.134089	48	7	26	17	2	0.42	0.48	70
40-1010	Maopu, Top	23.134089	52	5	24	18	1	0.41	0.75	57
43-1010	Chutouchi	23.133343	46	7	27	19	2	0.43	0.71	73
37-1109	Maopu Shale	23.08783	46	6	35	13	0	0.24	1.10	83
TN-01-08	Tangenshan	23.06182	45	5	33	15	0	0.29	-	-
18-1108	rezent	23.00832	71	2	14	13	0	0.29	0.37	67

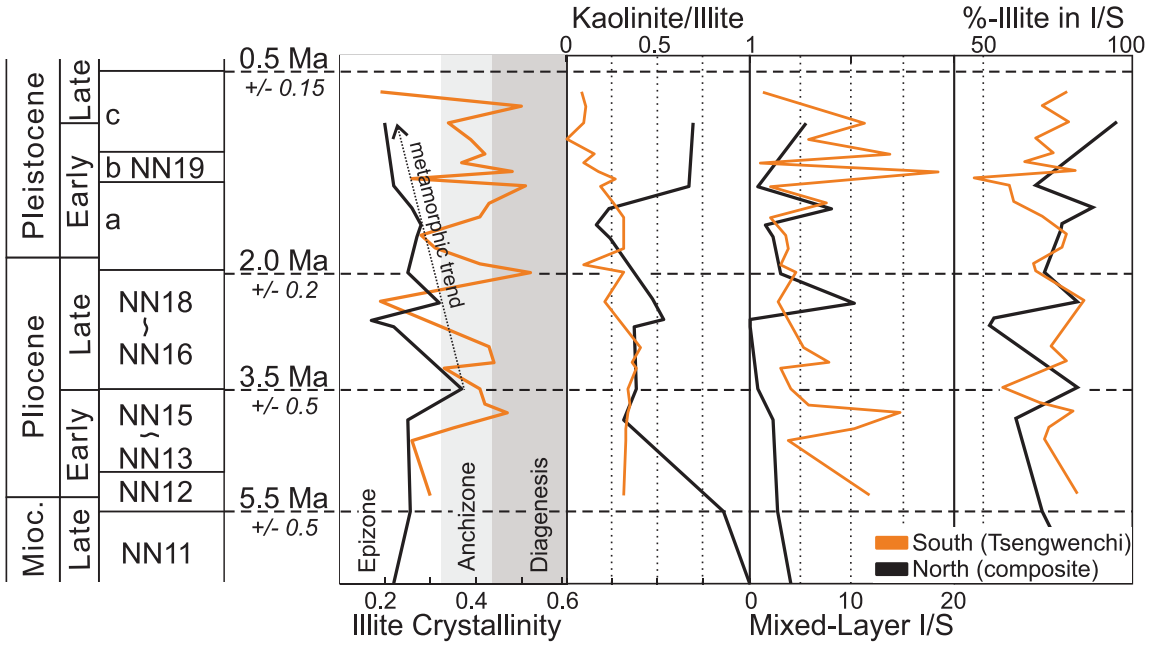

FIG. 9.—Variation of crystallinity index, kaolinite/illite ratio, mixed-layered illite/smectite (I/S), and percent illite in I/S. Composite section in the north (Dahanchi, Chuhuangkeng, Taanchi, Tsaohuchi, Nantou).

trajectories of burial and exhumation in the upper pro-wedge and retro-wedge (Willett 1999; Fuller et al. 2006; Sinclair 2012). In contrast, along the retro-side of the orogen (i.e., Coastal Range) the progressive temporal increase in low-grade metamorphic detritus up-section reflects exhumation and unroofing (Dorsey 1988), as confirmed by zircon fission-track data (Kirstein et al. 2009).

Illite crystallinity consistently increases up-section on the retro-side (Dorsey 1988). A similar but less clear trend is observed along the pro-side (i.e., Western Foothills), and is more pronounced in the north than in the south as a consequence of southward-propagating collisional shortening influenced by the pre-existing geometry and paleo-topography of colliding margins.

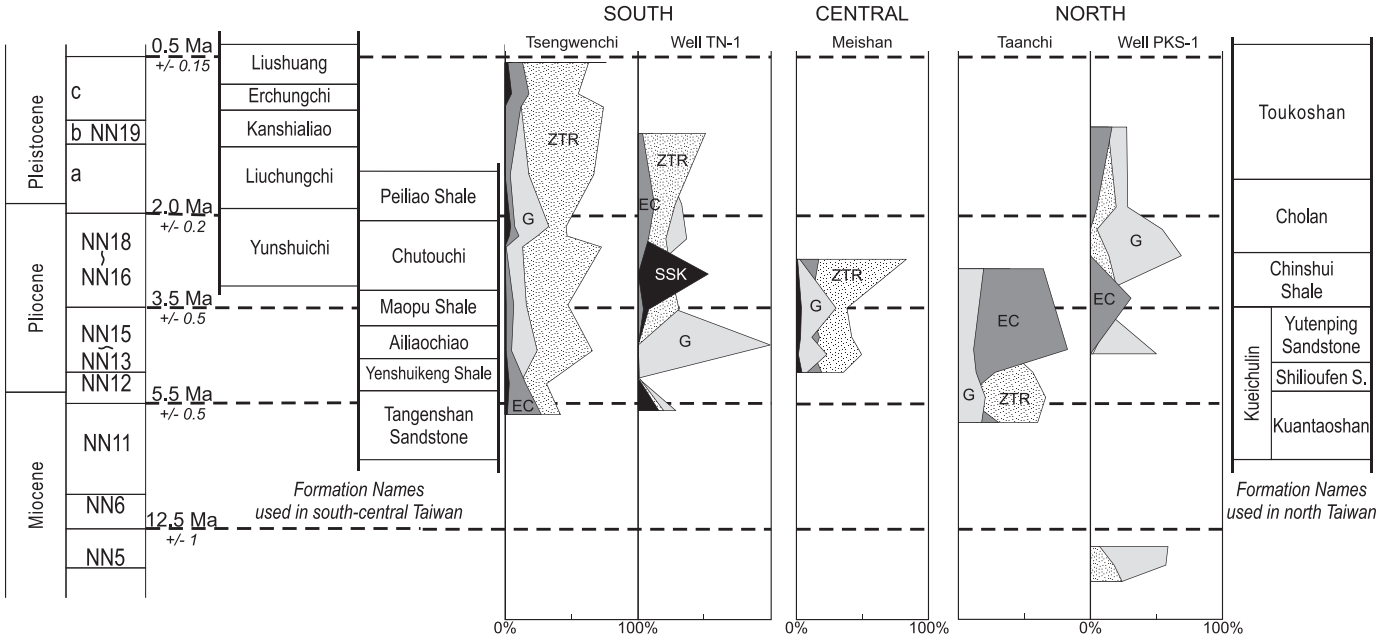

FIG. 10.—Simplified graph of heavy-mineral frequencies observed in sandstones (total 23 samples). Two boreholes from the south (TN-1) and the north (PKS-1) respectively show similar trends (Chou 1970; Chou 1971). ZTR, zircon, tourmaline, and rutile (ultrastable minerals); G, garnet; EC, epidote and chloritoid (low-grade metamorphic sources); SSK, sillimanite, staurolite, and kyanite (high-grade metamorphic sources). The Taanchi section shows a distinct up-section increase in epidote and chloritoid. The southern sections are dominated by the ultrastable ZTR association.

TABLE 4.—*Heavy-mineral analyses of the Taanchi (north), Meishan (central), and Tsengwenchi (south) sections. The Heavy Mineral Concentration Index (HMC) (Garzanti and Andò 2007) defines the abundance of heavy minerals in a sample (transparent, opaque, and unidentified turbid grains denser than 2.90 g/cm3). The ZTR Index (Hubert 1962) defines the maturity of the sediment. Samples with an asterisk (*) were analyzed at Università di Milano–Bicocca by M. Limonta. Samples analyzed in Milano were dry or wet sieved in order to eliminate both fine cohesive material (< 32 μm) and coarse fragments (> 355 μm). A size window of 3.5 ϕ was chosen for analysis. From the 32–355 μm class, the dense fraction was separated by centrifuging in sodium metatungstate (density(1986) ≈ 2.90 g/cm3) and recovered by partial freezing with liquid nitrogen. No chemical pre-treatment, which might have modified the original detrital assemblage in the laboratory, was used. About 200 transparent heavy minerals were counted in grain mounts by the "area method" (Galehouse 1971).*

Unit	Sample	HMC	% Transparent	% Opaque	% Turbid	Zircon	Tourmaline	Rutile	Ti Oxides	Apatite	Titanite	Others	Epidote	Garnet	Chloritoid	Staurolite	Kyanite	Sillimanite	Blue-green Hornblende	Brown Hornblende	& Amphiboles	Clinopyroxene	Enstatite	Hypersthene	Olivine	Spinel	MMI	ZTR
Modern (Taina n Beach)																												
Modern Beach	S4478*	0.5	16%	5%	79%	31	22	10	1	10	1	0	4	14	1	0	0	0	1	1	0	3	0	0.5	0	0.5	0	64
Modern Beach	S4479*	0.3	14%	7%	78%	33	22	8	0	9	2	0	7	10	0	2	0	0	0	0	0	6	0	0	0	1.1	33	63
Modern Beach	19-1108	0.2	5%	9%	86%	3	10	3	2	3	0	5	38	8	0	0	5	0	0	7	0	13	0	0	2	0.0	67	18
Tsengwen-chi																												
Liushuang *(lower)*	TWC-3808	0.4	35%	10%	55%	24	23	8	1	4	0	3	6	11	3	4	1	1	0	8	0	4	0	0	1	0.4	28	56
Erchungchi Fm *(upper)*	63-1010*	0.5	37%	7%	56%	47	21	7	0.5	4	1	0	5	12	0.5	0	0	0	0	0	0	0	0	0	0	0.5	n.d.	75
Liuchungchi Fm	53-1010*	0.4	26%	6%	68%	42	18	8	0	13	0	0	2	18	0	0	0	0	0	0	0	0	0	0	0	0	n.d.	67
Peiliao Shale	20-1108	0.4	38%	19%	44%	31	7	9	3	10	0	2	1	25	5	2	0	2	0	5	0	1	0	0	0	0	48	50
Yunshuichi Fm *(upper)*	47-1010*	0.4	39%	5%	57%	32	32	9	1	11	0	0.5	0	13	0	0	0	0	0	0	0	0	0	0	0	0	n.d.	75
Peiliao Shale	30-1108	0.2	21%	21%	58%	28	8	10	5	7	0	0.0	4	33	0	2	2	0	0	0	0	0	0	0	0	1	7	51
Chutouchi Fm	42-1010*	0.6	23%	3%	74%	11	28	9	2	30	0	0	0	16	3	1	0	0	0	0	0	0	0	0	0	0	8	50
Ailiaochiao Fm	36-1109*	0.1	31%	10%	59%	43	12	11	1	4	0	0	0	24	2	1	0	0	0	0	0	0	0	0	0	0	11	68
Yenshuikeng Shale *(lower)*	17-0109	0.2	16%	6%	77%	9	19	3	2	27	0	1	2	12	6	2	1	1	0	11	0	3	0	0	0	1	22	34
Tangenshan Sandstone *(upper)*	11-0109	0.1	13%	6%	82%	5	31	6	8	22	0	1	4	10	10	1	1	0	0	1	0	0	0	0	0	1	21	50
Taan-chi																												
Cholan Fm *(lower)*	27-1109*	0.3	32%	13%	54%	15	17	7	0.0	9	0	0	31	19	1	1	0	0	0	0	0	0	0	0	0	0	17	39
Chinsui Shale *(upper)*	29-1109*	1.3	23%	4%	72%	12	17	9	1.4	6	2	0	41	12	0.5	0	0	0	0	0	0	0	0	0	0	0	n.d.	39
Kueichulin Fm *(Yutengping Sandstone)*	25-1109*	0.6	40%	10%	50%	22	25	10	2.4	12	1	0	12	14	2	0	0	0	0	0	0	0	0	0	0	0	0	59
Kueichulin Fm *(Yutengping Sandstone)*	24-1109*	0.3	44%	10%	46%	38	19	9	0.9	10	0	0	3	21	0	0	0	0	0	0	0	0	0	0	0	0	n.d.	67
Kueichulin Fm *(Kuantaoshan Sandstone)*	30-1109*	0.3	36%	18%	46%	39	14	7	0.5	5	0	0.5	15	18	0	1	0	0	0	0	0	0	0	0	0	0	33	61
Meishan																												
Cholan (lower)	11-1108	0.3	26%	14%	60%	51	12	22	3.0	0	0	1	2	3	3	1	0	0	0	1	0	1	0	0	0	0	26	86
Kueichulin Fm *(Yutengping Sandstone)*	44-1108	0.2	22%	3%	76%	15	13	11	2.4	12	0	0	0	30	5	2	1	2	0	7	0	1	0	0	0	0	17	41
Kueichulin Fm *(Yutengping Sandstone)*	5-0109	0.3	30%	7%	64%	25	10	7	9.7	22	0	1	7	12	1	3	0	0	0	1	0	0	0	0	0	0.4	22	52
Kueichulin Fm *(Shilioufen Sandstone)*	5-1108	0.3	31%	7%	62%	26	16	7	2	11	0	0	5	23	2	1	0	0	0	3	0	2	0	0	0	1	29	52
Kueichulin Fm *(Kuantaoshan Sandstone)*	3-1108	0.2	21%	5%	74%	12	18	6	5	31	0	1	6	8	3	2	1	1	0	5	0	0	0	0	0	1	10	41

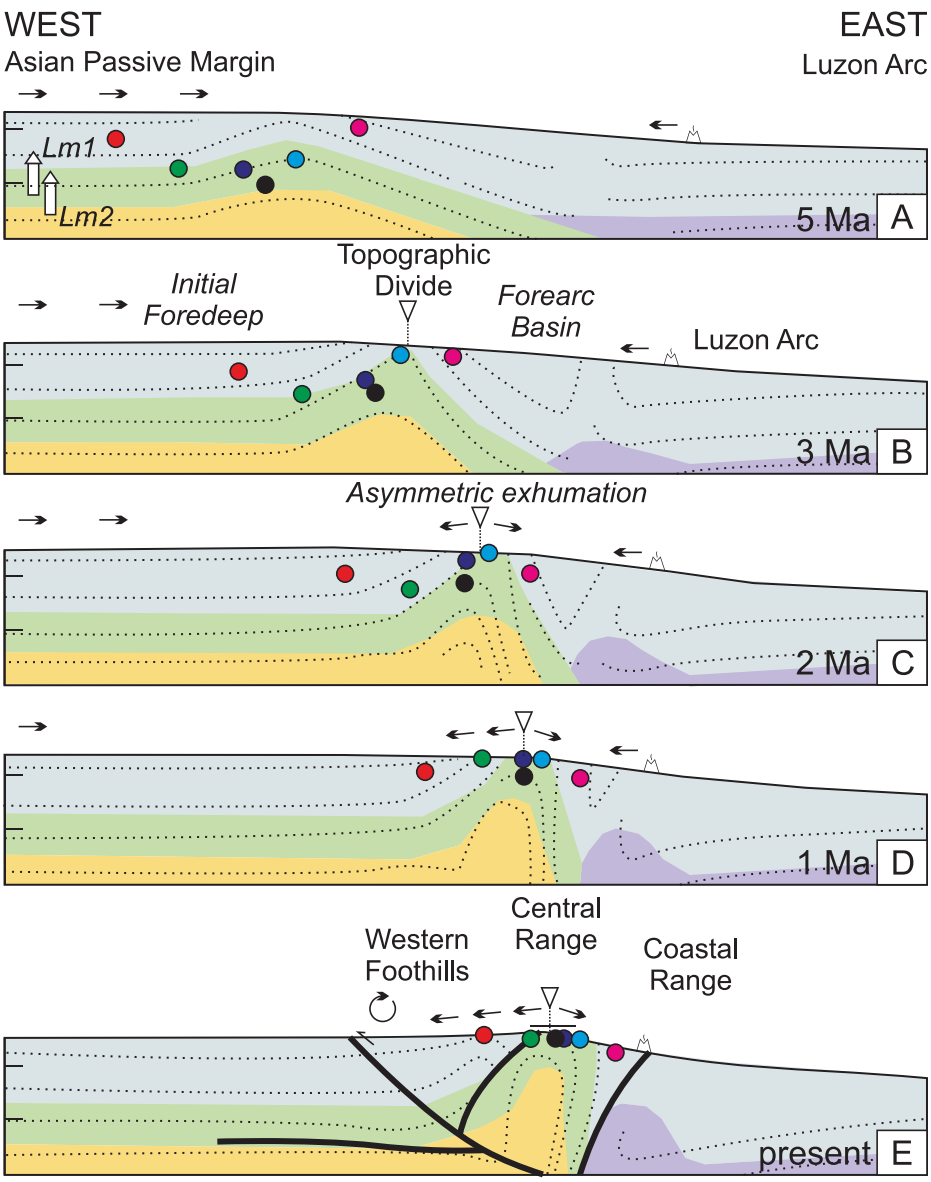

FIG. 11.—Schematic tectonic evolution of Taiwan from the early Pliocene to the present, based on the thermomechanical model of Yamato et al. (2009). Markers (colored dots) are all placed in the upper continental crust (particle flowlines shown as dotted lines) (Yamato et al. 2009) and illustrate exhumation of very low- (i.e., Lm_1) to low–medium-grade (i.e., Lm_2) metamorphic source rocks. Background colors refer to metamorphic facies zones calculated initially from the P-T conditions observed at present. Violet, blueschist; orange, amphibolite; green, greenschist; gray, zeolite–prehnite–pumpellyite. Note that at 3 Ma, metamorphic material begins to be exhumed in the subaerial wedge. Ongoing collision and subduction of the Asian continental margin creates a strongly asymmetric wedge, which controls distribution of sediment composition. Increased thrust activity at the deformation front increases recycling of the sedimentary cover of the wedge and obscures the metamorphic signal.

Heavy-mineral assemblages along the pro-foreland side suggest a relatively stable drainage area through time, with supply of sedimentary and subordinately metasedimentary detritus (e.g., stratigraphic section at Tsengwen-chi, 2 and 3 in Fig. 2). Deepening of the erosion level since the middle–late Pliocene is suggested in the north (e.g., Taan-chi section, 10 in Fig. 2).

This study demonstrates contrasting stratigraphic compositional trends documented on the pro-side and retro-side of a doubly-vergent orogenic wedge achieved since onset of collision. These opposite trends of recycling and unroofing, respectively, are held to be a diagnostic mark of the detrital record produced by erosion of asymmetric orogens formed during arc–continent collision.

ACKNOWLEDGMENTS

This paper stemmed from the first author's Ph.D. thesis work, supervised by S. Castelltort, University of Geneva, ETH Zurich. Many thanks for guidance and support. We thank the reviewers R. Ingersoll and J. Arribas, who thoroughly reviewed the manuscript; their criticisms and suggestions improved it immensely. We also thank Associate Editor Luiz Fernando De Ros. This project was funded by SNSF Swiss National Science Foundation Grant Number #200020-131890.

REFERENCES

ABBOTT, L.D., SILVER, E.A., THOMPSON, P.R., FILEWICZ, M.V., SCHNEIDER, C., AND ABDOERRIAS, 1994, Stratigraphic constraints on the development and timing of arc–continent collision in northern Papua New Guinea: Journal of Sedimentary Research, v. 64, p. 169–183.

ANDÒ, S., MORTON, A., AND GARZANTI, E., 2013, Metamorphic grade of source rocks revealed by chemical fingerprints of detrital amphibole and garnet, *in* Scott, R.A., Smyth, H.R., Morton, A.C., and Richardson, N., ed., Sediment Provenance Studies in Hydrocarbon Exploration and Production: Geological Society of London, Special Publication 386.

BARR, T.D., AND DAHLEN, F.A., 1989, Brittle frictional mountain building 2. Thermal structure and heat budget: Journal of Geophysical Research, v. 94, p. 3923–3947.

CASTELLTORT, S., NAGEL, S., MOUTHEREAU, F., LIN, A.T.-S., WETZEL, A., KAUS, B., D, W.S., CHIANG, S.-P., AND CHIU, W.-Y., 2011, Sedimentology of early Pliocene sandstones in the south-western Taiwan foreland: implications for basin physiography in the early stages of collision: Journal of Asian Earth Sciences, v. 40, p. 52–71.

CHANG, S.S.L., AND CHI, W.-R., 1983, Neogene nannoplankton biostratigraphy in Taiwan and the tectonic implications: Petroleum Geology of Taiwan, v. 19, p. 93–147.

CHEN, C.H., CHU, H.T., LIOU, J.G., AND ERNST, W.G., 1983, Explanatory Notes for the Metamorphic Facies Map of Taiwan, Central Geological Survey, Special Publication 2, 1–32 p.

Chen, W.-S., Ridgway, K.D., Horng, C.-S., Chen, Y.-G., Shea, K.-S., and Yeh, M.-G., 2001, Stratigraphic architecture, magnetostratigraphy and incised-valley systems of the Pliocene–Pleistocene collisional marine foreland basin Taiwan: Geological Society of America, Bulletin, v. 113, p. 1249–1271.

Chen, W.S., Erh, C.H., Chen, M.M., Yang, C.C., Chang, I.S., Liu, T.K., Horng, C.-S., Shea, K.-S., Yeh, M.-G., Wu, J.C., Ko, C.T.L., C.C., and Huang, N.W., 2000, The evolution of foreland basins in western Taiwan: evidence from the Plio-Pleistocene sequences: Central Geological Survey, Bulletin, v. 13, p. 137–156 (in Chinese with English abstract).

Chen, Z.H., Chen, W.S., Wang, Y., and Chen, M.M., 1992, Petrographicalstudy of foreland sandstones and its relation to unroofing history of the fold-thrust belt in central Taiwan: Ti-Chih, v. 12, p. 147–165 (in Chinese with English abstract).

Chi, W.-R., 1978, The late neogene nannobiostratigraphy in the Tainan foothills region, Southern Taiwan: Petroleum Geology of Taiwan, v. 15, p. 89–125.

Chou, J.-T., 1968, A stratigraphic and sedimentary analysis of the Protoquarzite in the Miocene Talu Shale in northern Taiwan: Petroleum Geology of Taiwan, v. 6, p. 115–138.

Chou, J.-T., 1970, A stratigraphic and sedimentary analysis of the miocene in Northern Taiwan: Petroleum Geology of Taiwan, v. 7, p. 145–189.

Chou, J.-T., 1971, A sedimentologic and paleogeographic study of the Neogene formations in the Taichung region, Western Taiwan: Petroleum Geology of Taiwan, v. 9, p. 43–66.

Chou, J.-T., 1973, Sedimentology and paleogeography of the upper Cenozoic system of Western Taiwan: Geological Society of China, Proceedings, v. 16, p. 111–143.

Chou, J.-T., 1976, A sedimentologic and paleogeographic study of the miocene Shihti formation in Western Taiwan: Petroleum Geology of Taiwan, v. 13, p. 119–138.

Covey, M., 1984, Sedimentary and Tectonic Evolution of the Western Taiwan Foredeep [Unpublished Ph.D. thesis]: Princeton University, 152 p.

Dahlen, F.A., and Suppe, J., 1988, Mechanics, growth, and erosion of mountain belts, *in* Clark, S.P., Burchfiel, B.C., and Suppe, J., eds., Processes in Continental Lithospheric Deformation: Geological Society of America, Special Paper 218, p. 161–178.

Davis, D., Suppe, J., and Dahlen, F.A., 1983, Mechanics of fold-and-thrust belts and accretionary wedges: Journal of Geophysical Research, v. 88, p. 1153–1172.

Decelles, P.G., 2011, Foreland basin systems revisited: variations in response to tectonic settings, *in* Azor, C.B.A., ed., Tectonics of Sedimentary Basins: Recent Advances: New York, John Wiley & Sons, p. 405–426.

Dickinson, W.R., 1970, Interpreting detrital modes of graywacke and arkose: Journal of Sedimentary Research, v. 40, p. 695–707.

Dickinson, W., 1985, Interpreting provenance relations from detrital modes of sandstones, *in* Zuffa, G.G., ed., Provenance of Arenites: NATO ASI Series, Springer, p. 333–361.

Dickinson, W.R., and Suczek, C.A., 1979, Plate tectonics and sandstone compositions: American Association of Petroleum Geologists, Bulletin, v. 63, p. 2164–2182.

Dorsey, R.J., 1988, Provenance evolution and unroofing history of a modern arc–continent collision: evidence from petrography of Plio-Pleistocene sandstones, Eastern Taiwan: Journal of Sedimentary Petrology, v. 58, p. 208–218.

Dorsey, R.J., and Lundberg, N., 1988, Lithofacies analysis and basin reconstruction of the Plio-Pleistocene collisional basin, Coastal Range of Eastern Taiwan: Acta Geologica Taiwanica, v. 26, p. 57–132.

Dorsey, R.J., Buchovecky, E.J., and Lundberg, N., 1988, Clay mineralogy of Pliocene–Pleistocene mudstones, eastern Taiwan: combined effects of burial diagenesis and provenance unroofing: Geology, v. 16, p. 944–947.

Ernst, W.G., 1983, Mineral parageneses in metamorphic rocks exposed along Tailuko Gorge, Central Mountain Range, Taiwan: Journal of Metamorphic Geology, v. 1, p. 305–329.

Fuller, C.W., Willett, S.D., Fisher, D., and Lu, C.Y., 2006, A thermomechanical wedge model of Taiwan constrained by fission-track thermochronometry: Tectonophysics, v. 425, p. 1–24.

Galehouse, J.S., 1971, Point counting, *in* Carver, R.E., ed., Procedures in Sedimentary Petrology: New York, Wiley, p. 385–407.

Garzanti, E., and Andò, S., 2007, Chapter 20, Heavy Mineral Concentration in Modern Sands: Implications for Provenance Interpretation, *in* Maria, A.M., and David, T.W., eds., Developments in Sedimentology: Amsterdeam, Elsevier, v. 58, p. 517–545.

Garzanti, E., and Vezzoli, G., 2003, A classification of metamorphic grains in sands based on their composition and grade: Journal of Sedimentary Research, v. 73, p. 830–837.

Ho, C.S., 1988, An introduction to the geology of Taiwan: explanatory text of the geologic map of Taiwan: Central Geological Survey, The Ministry of Economic Affairs, R.O.C. Taiwan, 192 p.

Horng, C.-S., Huh, C.-A., Chen, K.-H., Lin, C.-H., Shea, K.-S., and Hsiung, K.-H., 2012, Pyrrhotite as a tracer for denudation of the Taiwan orogen: Geochemistry, Geophysics, Geosystems, v. 13, p. Q08Z47.

Horng, C.-S., and Shea, K.-S., 1996, Dating of the Plio-Pleistocene rapidly deposited sequence based on integrated magnet-biostratigraphy: a case study of the Madagida–Chi section, Coastal Range, Eastern Taiwan: Geological Society of China, Journal, v. 39, p. 31–58.

Huang, A.H., Lin, A.T., Jiang, W.T., and Wu, R.Z., 2012, Clay mineralogy of the Miocene–Pleistocene sedimentary rocks, NW Taiwan: Western Pacific Earth Sciences, v. 12, p. 65–84 (in Chinese with English abstract and figure captions).

Huang, T.-C., 1976, Neogene calcareous nannoplankton biostratigraphy viewed from the Chuhuankeng section, NW Taiwan: Geological Society of China, Proceedings, v. 19, p. 7–24.

Huang, T., 1977, Late Neogene planktonic foraminiferal biostratigraphy of the Tainan Foothills region, Tainan, Taiwan: Petroleum Geology of Taiwan, v. 14, p. 121–145.

Huang, T., and Huang, T.-C., 1984, Neogene biostratigraphy of Taiwan, *in* Ikebe, N., and Tsuchi, R., eds., Pacific Neogene Datum Planes: Contributions to Biostratigraphy and Chronology: University of Tokyo Press, p. 288.

Hubert, J.F., 1962, A zircon-tourmaline-rutile maturity index and the interdependence of the composition of heavy mineral assemblages with the gross composition and texture of sandstones: Journal of Sedimentary Petrology, v. 32, p. 440–450.

Huh, C.-A., Chen, W., Hsu, F.-H., Su, C.-C., Chiu, J.-K., Lin, S., Liu, C.-S., and Huang, B.-J., 2011, Modern (< 100 years) sedimentation in the Taiwan Strait: rates and source-to-sink pathways elucidated from radionuclides and particle size distribution: Continental Shelf Research, v. 31, p. 47–63.

Ingersoll, R.V., and Suczek, C.A., 1979, Petrology and provenance of Neogene sand from Nicobar and Bengal fans, DSDP sites 211 and 218: Journal of Sedimentary Petrology, v. 49, p. 1217–1228.

Ingersoll, R.V., Bullard, T.F., Ford, R.L., Grimm, J.P., Pickle, J.D., and Sares, S.W., 1984, The effect of grain size on detrital modes; a test of the Gazzi–Dickinson point-counting method: Journal of Sedimentary Research, v. 54, p. 103–116.

Jahn, B.M., Martineau, F., Peucat, J.J., and Cornichet, J., 1986, Geochronology of the Tananao Schist complex, Taiwan, and its regional tectonic significance: Tectonophysics, v. 125, p. 103–124.

Kaus, B.J.P., Steedman, C., and Becker, T.W., 2008, From passive continental margin to mountain belt: insights from analytical and numerical models and application to Taiwan: Physics of the Earth and Planetary Interiors, v. 171, p. 235–251.

Kirstein, L.A., Fellin, M.G., Willett, S.D., Carter, A., Chen, Y.-G., Garverz, J.I., and Lee, D.C., 2009, Pliocene onset of rapid exhumation in Taiwan during arc–continent collision: new insights from detrital thermochronometry: Basin Research, v. 22, p. 270–285.

Koons, P.O., 1990, Two-sided orogen: Collision and erosion from the sandbox to the Southern Alps, New Zealand: Geology, v. 18, p. 679–682.

Kübler, B., 1987, Cristallinité de l'illite, méthodes normalisées de préparation, méthodes normalisées de mesure: Université de Neuchâtel, Institute de Géologie, Cahiers v. série ADX 1, p. 1–8.

Kübler, B., and Jaboyedoff, M., 2000, Illite crystallinity: Comptes Rendus de l'Académie des Sciences, Sciences de la Terre et des Planètes, v. 331, p. 75–89.

Liew, Y.-C., and Lin, C.A.-C., 1974, Heavy mineral association in the Neogene formation of the southern part of Coastal Range, East Taiwan: Acta Geologica Taiwanica, v. 17, p. 23–36.

Lin, A.T., and Watts, A.B., 2002, Origin of the West Taiwan basin by orogenic loading and flexure of a rifted continental margin: Journal of Geophysical Research, v. 107 (B9), p. 2185.

Lin, A.T., Watts, A.B., and Hesselbo, S.P., 2003, Cenozoic stratigraphy and subsidence history of the South China Sea margin in the Taiwan region: Basin Research, v. 15, p. 453–478.

Liu, Z., Tuo, S., Colin, C., Liu, J.T., Huang, C.-Y., Selvaraj, K., Chen, C.-T.A., Zhao, Y., Siringan, F.P., Boulay, S., and Chen, Z., 2008, Detrital fine-grained sediment contribution from Taiwan to the northern South China Sea and its relation to regional ocean circulation: Marine Geology, v. 255, p. 149–155.

Liu, Z., Colin, C., Li, X., Zhao, Y., Tuo, S., Chen, Z., Siringan, F.P., Liu, J.T., Huang, C.-Y., You, C.-F., and Huang, K.-F., 2010, Clay mineral distribution in surface sediments of the northeastern South China Sea and surrounding fluvial drainage basins: source and transport: Marine Geology, v. 277, p. 48–60.

Lock, J., 2007, Interpreting Low-temperature Thermochronometric Data in Fold-and-thrust Belts: an Example from the Western Foothills, Taiwan [Unpublished Ph.D. Thesis]: University of Washington, 219 p.

Manius, W.G., Covey, M., and Stallard, R., 1985, The effects of provenance and diagenesis on clay content and cristallinity in Miocene through Pleistocene deposits, Southwestern Taiwan: Petroleum Geology of Taiwan, v. 21, p. 173–185.

Meng, C.-Y., 1971, A conception of the evolution of the island of Taiwan and its bearing on the development of Western Neogene sedimentary basins: Petroleum Geology of Taiwan, v. 9, p. 241–258.

Molli, G., and Malavieille, J., 2011, Orogenic processes and the Corsica/Apennines geodynamic evolution: insights from Taiwan: International Journal of Earth Sciences, v. 100, p. 1207–1224.

Moore, D.M., and Reynolds, R.C., 1997, X-Ray Diffraction and the Identification and Analysis of Clay Minerals, Second Edition: Oxford, U.K., Oxford University Press, 396 p.

Mouthereau, F., and Lacombe, O., 2006, Inversion of the Paleogene Chinese continental margin and thick-skinned deformation in the Western Foreland of Taiwan: Journal of Structural Geology, v. 28, p. 1977–1993.

Mouthereau, F., Lacombe, O., Deffontaines, B., Angelier, J., and Brusset, S., 2001, Deformation history of the southwestern Taiwan foreland thrust belt: insights from tectono-sedimentary analyses and balanced cross-sections: Tectonophysics, v. 333, p. 293–322.

Mouthereau, F., Deffontaines, B., Lacombe, O., and Angelier, J., 2002, Variations along the strike of the Taiwan thrust belt: basement control on structural style, wedge geometry, and kinematics, *in* Byrne, T.B., and Liu, C.-S., eds., Geology and Geophysics of an Arc–Continent collision, Taiwan: Geological Society of America, Special Paper 358, p. 31–54.

Nagel, S., Castelltort, S., Wetzel, A., Willett, S.D., Mouthereau, F., and Lin, A.T., 2013, Sedimentology and foreland basin paleogeography during Taiwan arc continent collision: Journal of Asian Earth Sciences, v. 62, p. 180–204.

Najman, Y., Bickle, M., Garzanti, E., Pringle, M., Barfod, D., Brozovic, N., Burbank, D., and Ando, S., 2009, Reconstructing the exhumation history of the Lesser Himalaya, NW India, from a multitechnique provenance study of the foreland basin Siwalik Group: Tectonics, v. 28, p. TC5018, 1–15.

Page, B.M., and Suppe, J., 1981, The Pliocene Lichi Mélange of Taiwan: its plate-tectonic and olistostromal origin: American Journal of Science, v. 281, p. 193–227.

Pan, T.-S., 2011, A Study on Sedimentary Environments of Nanchuang Formation to Yangmei Formation along the Dahan River Section, Northwestern Taiwan [unpublished Master's thesis]: National Central University, Jhongli, 110 p.

Puigdefàbregas, C., Muñoz, J.A., and Vergés, J., 1992, Thrusting and foreland basin evolution in the southern Pyrenees, *in* McClay, K., ed., Thrust Tectonics: London, Chapman & Hall, p. 247–254.

Sibuet, J.-C., and Hsu, S.-K., 1997, Geodynamics of the Taiwan arc–arc collision: Tectonophysics, v. 274, p. 221–251.

Sibuet, J.-C., Hsu, S.-K., Shyu, C.-T., and Liu, C.S., 1995, Structural and kinematic evolutions of the Okinawa trough backarc basin, *in* Taylor, B., ed., Backarc Basins: Tectonics and Magmatism: New York, Plenum Press, p. 343–379.

Simoes, M., Avouac, J.P., Beyssac, O., Goffé, B., Farley, K.A., and Chen, Y.-G., 2007, Mountain building in Taiwan: a thermokinematic model: Journal of Geophysical Research, v. 112, no. B11405.

Sinclair, H., 2012, Thrust wedge/foreland basin systems, *in* Busby, C., and Azor, A., eds., Tectonics of Sedimentary Basins: New York, John Wiley & Sons, p. 522–537.

Stolar, D.B., Willett, S.D., and Montgomery, D.R., 2007, Characterization of topographic steady state in Taiwan: Earth and Planetary Science Letters, v. 261, p. 421–431.

Suppe, J., 1981, Mechanics of mountain-building and metamorphism in Taiwan: Geological Society of China, Memoirs, v. 4, p. 67–89.

Suppe, J., 1983, Geometry and kinematics of fault bend folding: American Journal of Science, v. 283, p. 684–721.

Suppe, J., 1984, Kinematics of arc–continent collision, flipping of subduction, and back-arc spreading near Taiwan: Geological Society of China, Memoirs, v. 6, p. 21–33.

Suppe, J., and Namson, J., 1979, Fault-bend origin of frontal folds the western Taiwan fold and thrust belt: Petroleum Geology of Taiwan, v. 16, p. 1–18.

Tang, C.H., 1977, Late Miocene erosional unconformity on the subsurface Peikang high beneath the Chiayi–Yunlin coastal plain,Taiwan: Geological Society of China, Memoirs, v. 2, p. 155–167.

Teng, L.S., 1979, Petrographical study of Neogene sandstones of the Coastal Range, eastern Taiwan (1. Northern Part): Acta Geologica Taiwanica, v. 20, p. 129–155.

Teng, L.S., 1990, Geotectonic evolution of late Cenozoic arc–continent collision in Taiwan: Tectonophysics, v. 183, p. 57–76.

Tensi, J., Mouthereau, F., and Lacombe, O., 2006, Lithospheric bulge in the West Taiwan Basin: Basin Research, v. 18, p. 277–299.

Ting, H.-H., Huang, C.-Y., and Wu, L.-C., 1991, Paleoenvironments of the late Neogene sequences along the Nantzuhsien river, Southern Taiwan: Petroleum Geology of Taiwan, v. 26, p. 121–149.

Wan, S., Li, A., Clift, P.D., Wu, S., Xu, K., and Li, T., 2010, Increased contribution of terrigenous supply from Taiwan to the northern South China Sea since 8.5 Ma: Marine Geology, v. 278, p. 115–121.

Warr, L.N., and Rice, A.H.N., 1994, Interlaboratory standardization and calibration of clay mineral crystallinity and crystallite size data: Journal of Metamorphic Geology, v. 12, p. 141–152.

White, N.M., Pringle, M., Garzanti, E., Bickle, M., Najman, Y., Chapman, H., and Friend, P., 2002, Constraints on the exhumation and erosion of the high Himalayan slab, NW India, from foreland basin deposits: Earth and Planetary Science Letters, v. 195, p. 29–44.

Willett, S.D., 1999, Orogeny and orography: the effect of erosion on the structure of mountain belts: Journal of Geophysical Research, v. 104, p. 28,957–28,981.

Willett, S.D., and Brandon, M.T., 2002, On steady state in mountains belts: Geology, v. 30, p. 175–178.

Willett, S., Beaumont, C., and Fullsack, P., 1993, Mechanical model for the tectonics of doubly vergent compressional orogens: Geology, v. 21, p. 371–374.

Willett, S.D., Fisher, D., Fuller, C., En-Chao, Y., and Chia-Yu, L., 2003, Erosion rates and orogenic-wedge kinematics in Taiwan inferred from fission-track thermochronometry: Geology, v. 31, p. 945–948.

Wu, F.-T., 1967, Petrographic study of oil sands of the Mushan and the Wuchihshan Formation in the vicinity of Miaoli: Petroleum Geology of Taiwan, v. 5, p. 45–61.

Wu, L.-C., and Wang, Y., 1989, Depositional environments of the upper Miocene to lower Pleistocene series in the Yunshui-chi section, Chiayi area, Taiwan: Ti-Chih, v. 9, p. 15–44.

Yamato, P., Mouthereau, F., and Burov, E., 2009, Taiwan mountain building: insights from 2-D thermomechanical modelling of a rheologically stratified lithosphere: Geophysical Journal International, v. 176, p. 307–326.

Yang, T.F., Tien, J.-L., Chen, C.-H., Lee, T., and Punongbayan, R.S., 1995, Fission-track dating of volcanics in the northern part of the Taiwan–Luzon Arc: eruption ages and evidence for crustal contamination: Journal of Southeast Asian Earth Sciences, v. 11, p. 81–93.

Yen, J.-Y., and Lundberg, N., 2006, Sediment compositions in offshore southern Taiwan and their relations to the source rocks in modern arc–continent collision zone: Marine Geology, v. 225, p. 247–263.

Yu, H.-S., and Chou, Y.-W., 2001, Characteristics and development of the flexural forebulge and basal unconformity of western Taiwan foreland Basin: Tectonophysics, v. 333, p. 277–291.

Yu, N.-T., Teng, L.S., Tai, P.-C., and Yue, L.-F., 1999, Relative sea-level changes in Oligocene to Miocene strata in Northern Taiwan: a preliminary study: Geological Society of China, Journal, v. 42, p. 189–208.

Yu, N.-T., Teng, L.S., Chen, W.-S., and Yen, I.-C., 2008, Facies characteristics of the upper-Neogene Nantzuhsienchi Section, Kaohsiung, SW Taiwan: Petroleum Geology of Taiwan, v. 38, p. 30–56.

Received 20 August 2013; accepted 12 February 2014.